

Cite this: *Dalton Trans.*, 2025, **54**,  
16475

# Simulant chemistry for uranium and plutonium molten fuel salts: crystallographic investigation and thermodynamic modelling assessment of the NaCl–RECl<sub>3</sub> and NaCl–MgCl<sub>2</sub>–RECl<sub>3</sub> (RE = Ce, Nd) systems

Dennis C. Alders,<sup>a</sup> Ana Sacristán-Civera,<sup>a</sup> Mädchen Wolff,<sup>a</sup> Elisa Capelli,<sup>d</sup>  
Eleanor L. Bright,<sup>b,c</sup> Christoph Hennig,<sup>b,c</sup> Rudy J. M. Konings<sup>a</sup> and A. L. Smith<sup>b,\*</sup>

In this study, new insights into the solid state chemistry of the systems NaCl–RECl<sub>3</sub> (RE = Ce, Nd) are presented, in which the intermediate compound suggested in the literature, *i.e.* Na<sub>3</sub>RE<sub>5</sub>Cl<sub>18</sub>, is investigated more closely. Our studies have revealed a solubility range around the intermediate composition in the form of the Na<sub>3/2</sub>RE<sub>1–2/3</sub>Cl<sub>3</sub> stoichiometry, and have allowed us to revisit the phase diagrams of the NaCl–RECl<sub>3</sub> (RE = Ce, Nd) systems accordingly. Furthermore, we demonstrate that among the lanthanide chlorides, NdCl<sub>3</sub> is the prime simulant candidate for the melting behaviour of PuCl<sub>3</sub>-based systems, while CeCl<sub>3</sub> is most suited to simulate UCl<sub>3</sub>-based systems. This is corroborated in this work by comparing the melting profiles of the NaCl–MCl<sub>3</sub>, MgCl<sub>2</sub>–MCl<sub>3</sub>, and NaCl–MgCl<sub>2</sub>–MCl<sub>3</sub> (M = Ce, Nd, U, Pu) systems. In doing so, the binary systems MgCl<sub>2</sub>–MCl<sub>3</sub> (M = Ce, Nd) have been re-visited based on existing data in the literature and estimated mixing enthalpies. Extrapolations to the ternary systems NaCl–MgCl<sub>2</sub>–RECl<sub>3</sub> (RE = Ce, Nd) have been made and compared to the available data in the literature, showing good agreement.

Received 24th June 2025,  
Accepted 8th October 2025

DOI: 10.1039/d5dt01486g

rsc.li/dalton

## 1 Introduction

Molten chloride salts are a class of materials that are central in the development of fast neutron spectrum Molten Salt Reactor (MSR) development. In this type of nuclear reactor, chloride salts can be used as both fuel and coolant. The reason for this lies in their attractive qualities, notably their high thermochemical stability and low vapour pressures, even at elevated temperatures, and their high actinide solubility.<sup>1,2</sup> For a safety assessment of the MSR, a thorough understanding of the thermodynamic and thermo-physical properties of the fuel salts is needed. Salt systems that have garnered interest as candidate fuels are the systems NaCl–PuCl<sub>3</sub>,<sup>3</sup> NaCl–UCl<sub>3</sub>,<sup>4</sup> and NaCl–MgCl<sub>2</sub>–PuCl<sub>3</sub>,<sup>5–7</sup> with this work focussing mainly on the latter fuel system. Since there is a dearth of available experi-

mental data on the systems with PuCl<sub>3</sub> in general, additional data are urgently needed to assist the safety assessment of the molten chloride reactor. At this stage of MSR development, the amounts of PuCl<sub>3</sub> available for research are limited as it needs to be produced in special facilities due to its hazardous nature. Therefore, using an approach that does not involve the use of PuCl<sub>3</sub> may be desirable to reduce the number of necessary experiments. In particular, a close inspection of the (conflicting) available data in simulant systems with lanthanide elements is meaningful. In this work, we have scrutinized systems with lanthanide chlorides from La to Yb (and Y) to identify the elements whose behaviour is closest to that of the actinides in molten chloride salts, and to identify the most suitable simulant for the melting behaviour of PuCl<sub>3</sub>-based systems. We have found that NdCl<sub>3</sub> and CeCl<sub>3</sub> are the closest surrogates for NaCl–AnCl<sub>3</sub>, MgCl<sub>2</sub>–AnCl<sub>3</sub> and NaCl–MgCl<sub>2</sub>–AnCl<sub>3</sub> (An = U, Pu) systems, thereby calling for a close inspection of the corresponding rare earth chloride systems.

Experimental investigations using X-ray diffraction (XRD) have been performed to fill in important gaps that became evident after analyzing the data in the literature, *i.e.* related to the solid-state chemistry in the NaCl–RECl<sub>3</sub> systems. There is no single interpretation of the stable intermediate compounds in these systems, with some authors claiming a stoichiometry

<sup>a</sup>Delft University of Technology, Faculty of Applied Sciences, Radiation Science Technology Department, Mekelweg 15, 2629 JB Delft, The Netherlands.  
E-mail: a.l.smith@tudelft.nl

<sup>b</sup>The Rossendorf Beamline (BM20), European Synchrotron Radiation Facility, 71 Av. des Martyrs, 38000 Grenoble, France

<sup>c</sup>Helmholtz-Zentrum Dresden-Rossendorf, Institute of Research Ecology, Bautzner Landstraße 400, 01314 Dresden, Germany

<sup>d</sup>Orano Support, 92320 Châtillon, France



of  $\text{NaRE}_3\text{Cl}_{10}$ ,<sup>8,9</sup>  $\text{Na}_3\text{RE}_5\text{Cl}_{18}$ <sup>10,11</sup> or  $\text{Na}_{2x}(\text{Na}_x\text{RE}_{2-x})\text{Cl}_{16}$ ,<sup>12,13</sup> with the latter indicating possible solid solubility. Subsequently, CALPHAD models of the binary sub-systems  $\text{NaCl-NdCl}_3$  and  $\text{NaCl-CeCl}_3$  have been developed. The thermodynamic models use the quasi-chemical formalism in the quadruplet approximation for the liquid solutions, and a one-lattice polynomial model for the solid solutions. Moreover, the systems  $\text{MgCl}_2\text{-MCl}_3$  ( $M = \text{Ce, Nd, U, Pu}$ ) were modelled based on the available phase diagram data in the literature, and estimated mixing enthalpy data using the method of Davis and Rice,<sup>14</sup> as described in more detail in a previous work.<sup>15</sup> This allowed us to consider more generally the similarities in the  $\text{NaCl-MgCl}_2\text{-MCl}_3$  ( $M = \text{Ce, Nd, U, Pu}$ ) systems.

## 2 Methods

### 2.1 Experimental techniques

**2.1.1 Sample preparation.** For the experiments carried out in this work, the end-members  $\text{NaCl}$ ,  $\text{NdCl}_3$  and  $\text{CeCl}_3$  were used in their respective ultra-dry forms, as delivered by the supplier. The purity has been verified by X-Ray diffraction (XRD) and Differential Scanning Calorimetry (DSC), as shown in Table 1. No secondary impurity phases were detected, and the measured melting temperatures were found in excellent agreement with the data in the literature. Due to the sensitivity of the salts towards oxygen and water, all sample preparation was carried out inside a glove box under dry argon atmosphere ( $\text{H}_2\text{O}$ ,  $\text{O}_2 < 5$  ppm).

Weighing was carried out using a Mettler-Toledo XPE105DR balance with a 0.01 mg uncertainty. Sample preparation was conducted by mixing end-members in the appropriate stoichiometric ratios in an agate mortar inside the dry argon atmosphere in the glovebox. The sample containers were either nickel liners in stainless steel crucibles, also used in our previous works,<sup>15,18,19</sup> or vacuum-sealed borosilicate ampoules. Subsequently, the mixtures were subjected to a heat treatment for 48 h at  $T = 693$  K, either in a tubular furnace under argon flow or in a chamber furnace under air.

**2.1.2 Quenching experiments.** The high-temperature stability of the intermediate compound in the  $\text{NaCl-CeCl}_3$  and  $\text{NaCl-NdCl}_3$  systems was investigated in this work using quenching experiments. The quenching samples consisted of stoichiometric mixtures of the end-members, thoroughly mixed using a pestle and mortar before insertion inside a nickel liner in a tightly closed stainless steel crucible. During the experiments, the samples were heated to a temperature of 773 K and equilibrated at this temperature for at least two

hours, after which they were dropped into a water bath to freeze the phases stable at high temperature. No difference in obtained XRD pattern was observed when quenching after 4 hours of heat treatment instead of 2.

The furnace used for quenching was an MTI split vertical quenching tube furnace (OTF-1500X-80-VTQ), which contained an electromagnet that held the sample in the heated part of the furnace. When the sample was at the desired temperature and had reached equilibrium, the electromagnet was shut off and the sample dropped into a water bath. Due to the double containment of the sample of nickel inside stainless steel, the sample stayed water-free during this experiment.

#### 2.1.3 X-ray diffraction (XRD)

**Laboratory XRD.** XRD measurements were carried out using a PANalytical X'pert pro diffractometer with a Cu-anode (0.4 mm  $\times$  12 mm line focus, 45 kV, 40 mA). Scattered X-ray intensities were measured with a real-time multi-step detector (X'Celerator). The angle  $2\theta$  was set to cover a range from  $10^\circ$  to  $120^\circ$ . Measurements were typically performed for 7–8 hours, with a step size of  $0.0036^\circ \text{ s}^{-1}$ . Refinement of the measured XRD data was performed by applying the method of Rietveld, Loopstra and van Laar,<sup>20,21</sup> using the FullProf software, Version 5.10.<sup>22</sup> Visualisation of the crystal structure based on the refined XRD data was done with the VESTA software.<sup>23</sup>

**Synchrotron XRD.** In addition to XRD measurements obtained in our lab, high resolution synchrotron XRD (sXRD) measurements were performed. The resolution of synchrotron diffraction,  $\delta d/d$ , is  $1\text{--}2 \times 10^{-3}$  (depending on the capillary diameter, scattering angle and excitation energy), and thus typically a magnitude better than that of the lab diffractometer. It was used to investigate small impurities or additional phases that would otherwise be invisible on an XRD. The sXRD measurements were performed at the XRD-1 station of the ROBL beamline (BM20) at the ESRF.<sup>24</sup> This station was equipped with a 6-circle diffractometer and a Eiger CdTe 500k detector (Dectris). The wavelength of the synchrotron radiation was  $\lambda = 0.76533 \text{ \AA}$ , and the beam size was  $300 \times 300 \mu\text{m}$ . The sample was enclosed in a  $300 \mu\text{m}$  diameter glass capillary sealed with epoxy glue itself enclosed inside a Kapton tube. Data were collected in transmission mode at 296 K and reduced using the PyFAI software suite.<sup>25</sup> Data were collected from  $0 \leq 2\theta \leq 66^\circ$ . Refinement of the measured XRD data was also performed by applying the method of Rietveld, Loopstra and van Laar,<sup>20,21</sup> using the FullProf software, Version 5.10.<sup>22</sup>

### 2.2 Thermodynamic modelling

The thermodynamic modelling assessment of the molten salt systems was performed with the CALPHAD method<sup>26</sup> using the

**Table 1** Pure compounds used in the experiments in this work

Compound	Supplier	CAS No	Reported purity	Melting point (DSC, K)	Melting point (lit., K)
$\text{NaCl}$	Merck	7647-14-5	99.998%	$1074 \pm 5$	$1074 \pm 1^{16}$
$\text{NdCl}_3$	Thermo-Fischer	10024-93-8	99.99%	$1031 \pm 5$	$1030 \pm 2^{17}$
$\text{CeCl}_3$	Alfa Aesar	7790-86-5	99.9%	$1087 \pm 5$	$1090 \pm 2^{17}$



FactSage software, Version 8.2.<sup>27</sup> Both literature and experimental data obtained in this work were used to optimize the excess parameters of the Gibbs energy functions of the phases present in the systems.

**2.2.1 Stoichiometric compounds.** The Gibbs energy function for stoichiometric compounds is dependent on the standard enthalpy of formation ( $\Delta_f H_m^\circ(298)$ ), the standard entropy ( $S_m^\circ(298)$ ) at the reference temperature of 298.15 K and the heat capacity ( $C_{p,m}^\circ(T)$ ) as shown in eqn (1) (with  $T$  in K).

$$G(T) = \Delta_f H_m^\circ(298) - S_m^\circ(298)T + \int_{298}^T C_{p,m}^\circ(T) dT - T \int_{298}^T \frac{C_{p,m}^\circ(T)}{T} dT \quad (1)$$

The isobaric heat capacity  $C_{p,m}$  is expressed as a polynomial that takes the form of eqn (2).

$$C_{p,m}(T) = a + bT + cT^{-2} + dT^2 + eT^{1/2} \quad (2)$$

The thermodynamic data for all compounds are listed in Table 2. To be consistent with previous works<sup>15,18,19,28–30</sup> and the JRC Molten Salt Database,<sup>31</sup> thermodynamic data for  $MgCl_2$  were taken from the JANAF thermochemical database,<sup>16</sup> the thermodynamic data for  $NaCl$  was taken from van Oudenaren *et al.*,<sup>32</sup> and the thermodynamic data for  $CeCl_3$  and  $NdCl_3$  were taken from the review by Konings and Kovács.<sup>17</sup> The thermodynamic data for  $PuCl_3$  and  $UCl_3$  were taken from the review by Capelli and Konings,<sup>33</sup> with the heat capacity of  $UCl_3$  taken from the re-assessment by van Oudenaren *et al.*<sup>32</sup> The thermodynamic model of the  $NaCl$ – $MgCl_2$  system was presented in a previous work<sup>18</sup> and is used in this work as such.

**2.2.2 Liquid solution.** The excess Gibbs energy terms of the liquid solution are modelled using the quasi-chemical formalism in the quadruplet approximation as proposed by Pelton *et al.*<sup>36</sup> which has proven to be well-adapted to molten chloride and fluoride systems. This description assumes the existence of cation–anion quadruplets in the liquid, *i.e.* in the form of  $A-X-B-Y$  ( $A, B =$  cations;  $X, Y =$  anions), allowing for the modelling of short-range ordering. This formalism allows for the selection of the composition of maximum short-range ordering through its coordination numbers, corresponding to the minimum of the Gibbs energy that is often found near the composition of the lowest eutectic. By fixing either the cation–cation or anion–anion coordination number, the opposite coordination number is also obtained through eqn (3), where  $q_i$  are the charges of the respective ions. In this work, we can simplify the description to the  $A-X-B-X$  quadruplet as chlorine is the only anion we consider. The coordination numbers used in the thermodynamic model presented in this work are given in Table 3.

$$\frac{q_A}{Z_{AB/XX}^A} + \frac{q_B}{Z_{AB/XX}^B} = 2 \frac{q_X}{Z_{AB/XX}^X} \quad (3)$$

The excess parameters that are optimized are those related to the second-nearest neighbour exchange reactions as given in eqn (4). The associated change in Gibbs energy of eqn (4) is expressed in eqn (5).

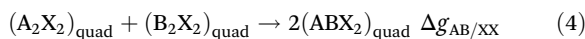
**Table 2** Thermodynamic functions used in the CALPHAD model in this work. Optimized values are marked in bold. Note that compounds marked with an asterisk are not stoichiometric intermediates, but rather end-members of the  $Na_{3x}RE_{2-x}Cl_6$  solid solution as specified in section 2.2.3

Compound	$\Delta_f H_m^\circ(298)$ (J mol <sup>-1</sup> )	$S_m^\circ(298)$ (J K <sup>-1</sup> mol <sup>-1</sup> )	$C_{p,m}(T)$ (J K <sup>-1</sup> mol <sup>-1</sup> ) = $a + bT + cT^{-2} + dT^2 + eT^{1/2}$					Temperature range (K)	Source
			a	b	c	d	e		
NaCl(s)	-411 260	72.15	47.72158	0.0057	-882.996	1.21466 × 10 <sup>-5</sup>		298–1074	van Oudenaren <i>et al.</i> <sup>32</sup>
NaCl(l)	-390 852.5	83.302	68					298–2500	Dumaire <i>et al.</i> <sup>28</sup>
MgCl <sub>2</sub> (s)	-641 616	89.629	54.5843	0.0214213	-1 112 119	-2.3567 × 10 <sup>-6</sup>		298–2000	Chase <i>et al.</i> <sup>16</sup>
MgCl <sub>2</sub> (l)	-601 680.1	129.236	193.4089	-0.3620139	-3 788 504	3.199871 × 10 <sup>-4</sup>		298–660	Chase <i>et al.</i> <sup>16</sup>
CeCl <sub>3</sub> (s)	-1 059 700	151	90.9772	0.0358123	-271 530			660–2500	Chase <i>et al.</i> <sup>16</sup>
CeCl <sub>3</sub> (l)	-1 006 100	151	90.9772	0.0358123	-271 530			298–1095	Konings and Kovács <sup>17</sup>
NdCl <sub>3</sub> (s)	-1 040 900	153.5	109.084	1.6406 × 10 <sup>-2</sup>	-1 309 950			298–1095	Konings and Kovács <sup>17</sup>
NdCl <sub>3</sub> (l)	-1 017 943.3	154.59	150					298–1095	Konings and Kovács <sup>17</sup>
PuCl <sub>3</sub> (s)	-959 600	161.4	91.412	0.03716				1095–3000	Konings and Kovács <sup>17</sup>
PuCl <sub>3</sub> (l)	-931 116	170.46	144			27 400		298–1032	Konings and Kovács <sup>17</sup>
UCl <sub>3</sub> (s)	-863 700	163.9	106.967	-0.0208595	-129 994			298–1032	Konings and Kovács <sup>17</sup>
UCl <sub>3</sub> (l)	-846 616	152.919	151.1					1095–3000	Konings and Kovács <sup>17</sup>
NaMgCl <sub>3</sub> (s)	-1 063 200	156	90	0.075				298–1500	Capelli and Konings <sup>33</sup>
Na <sub>2</sub> MgCl <sub>4</sub> (s)	211	111.25	135	0.1125				298–1100	Capelli and Konings <sup>33</sup>
Na <sub>6</sub> MgCl <sub>8</sub>	-3 148 000	481.5	340.9138	0.055621	-1 117 417			1100–2500	van Oudenaren <i>et al.</i> <sup>32</sup>
Na <sub>2</sub> Mg <sub>5</sub> Cl <sub>8</sub>	-2 767 200	410	252.3333	0.059943	-2 226 887			298–1000	Chartrand <i>et al.</i> , <sup>34</sup> Alders <i>et al.</i> <sup>18</sup>
NaNdCl <sub>7</sub> *	-2 505 000	378.5	265.88958	0.038512	-2 620 782.996			298–773	Chartrand <i>et al.</i> , <sup>34</sup> Alders <i>et al.</i> <sup>18</sup>
NaCeCl <sub>7</sub> *	-2 542 000	374.15	229.676	0.0773246	-543 882.996			298–6000	Alders <i>et al.</i> <sup>18</sup>
NaU <sub>2</sub> Cl <sub>7</sub>	-2 112 623	438	261.65558	-0.036019	-260 870.996			298–1500	This work
								298–1500	Yingling <i>et al.</i> , <sup>35</sup> This work



**Table 3** Non-default coordination numbers used in the CALPHAD model presented in this work

A	B	X	Z <sub>AB/XX</sub> <sup>A</sup>	Z <sub>AB/XX</sub> <sup>B</sup>	Z <sub>AB/XX</sub> <sup>X</sup>	Source
Na	Mg	Cl	3	6	3	18
Na	Nd	Cl	4	6	2.67	This work
Na	Ce	Cl	3	6	2.4	This work
Na	U	Cl	2	6	2	35
Na	Pu	Cl	3	6	2.4	28
Mg	Ce	Cl	3	6	1.71	This work
Mg	U	Cl	3	6	1.71	This work



$$\Delta g_{AB/XX} = \Delta g_{AB/XX}^{\circ} + \sum_{i \geq 1} g_{AB/XX}^{i\circ} \chi_{AB/XX}^i + \sum_{j \geq 1} g_{AB/XX}^{j\circ} \chi_{BA/XX}^j \quad (5)$$

In eqn (5) the terms  $\Delta g_{AB/XX}^{\circ}$ ,  $\Delta g_{AB/XX}^{i\circ}$  and  $\Delta g_{AB/XX}^{j\circ}$  are composition-independent coefficients that may depend on temperature. The composition dependence of the Gibbs energy is apparent through  $\chi_{AB/XX}$  as these are defined as per eqn (6). In this equation  $X_{AA}$  is the cation-cation pair fraction, or the molar fraction of the quadruplet containing two cations A. For this binary system,  $\{X_{AA} + X_{AB} + X_{BB}\}$  is equal to one.

$$\chi_{AB/XX} = \frac{X_{AA}}{X_{AA} + X_{AB} + X_{BB}} \quad (6)$$

The Gibbs energy functions used in this work to describe the liquid solutions are given in Table 4. Using the data for the binary systems as a basis, extrapolations to the ternary and quaternary fields were made with Kohler/Toop interpolations, due to the asymmetry of the system. In this work, MgCl<sub>2</sub>, CeCl<sub>3</sub> and NdCl<sub>3</sub> are considered asymmetric components, as their ionic structure in the liquid (*i.e.* molecular species) is different from the sodium halides (*i.e.* ionic species). No ternary optimization terms were added, to be consistent with the work of Beneš *et al.*<sup>37</sup>

**2.2.3 Solid solution modelling of Na<sub>3x</sub>RE<sub>2-x</sub>Cl<sub>6</sub>.** The thermodynamic description of solid-solutions is done using the one-lattice polynomial model to be consistent with the

**Table 5** Optimized excess Gibbs energy functions used in the CALPHAD model in this work for the solid solution

A	B	L <sub>AB</sub> <sup>11</sup>
NaCl	NaCe <sub>2</sub> Cl <sub>7</sub>	-9000 + 15 T
NaCl	NaNd <sub>2</sub> Cl <sub>7</sub>	-6500 + 7.5 T

description of the JRC Molten Salt Database (JRCMSD).<sup>31</sup> The Gibbs Energy function of the solid-solution is given in eqn (7).

$$G(T) = X_A \cdot G_A^{\circ} + X_B \cdot G_B^{\circ} + X_A RT \ln X_A + X_B RT \ln X_B + \Delta G_m^{\text{excess}} \quad (7)$$

In the above equation,  $G_i^{\circ}$  are the end-member molar Gibbs energies, and  $X_i$  are the site molar fractions of the end-members A and B, respectively. The third and fourth terms in eqn (7) represent the configurational entropy. The excess Gibbs energy, present in eqn (7) as  $\Delta G_m^{\text{excess}}$ , is defined as per eqn (8).

$$\Delta G_m^{\text{excess}} = \sum_{ij \geq 1} X_A^i X_B^j L_{AB}^{ij} \quad (8)$$

The term  $L_{AB}^{ij}$  in eqn (8) is an interaction coefficient that can be a function of temperature if necessary. The terms  $X_A^i$  and  $X_B^j$  are the site molar fractions of end-members A and B. To model the homogeneity range of the Na<sub>3x</sub>RE<sub>2-x</sub>Cl<sub>6</sub> intermediate, the NaCl and NaRE<sub>2</sub>Cl<sub>7</sub> end-members were selected in this work. It is important to note that the Gibbs energy of the NaCl end-member was also destabilised with an arbitrary enthalpic term of +5000 J mol<sup>-1</sup> to be able to reproduce accurately the phase diagram data. The corresponding Gibbs energy functions are given in Table 5.

## 3 Results and discussion

### 3.1 Simulant selection

Cerium has often been cited as actinide surrogate in the literature,<sup>38-41</sup> but other rare earth elements show comparable behaviour. Cerium is commonly used for the fact that its stable oxidation states (*i.e.* +3 and +4) mirror that of plutonium

**Table 4** Excess Gibbs energy functions used in the CALPHAD model in this work for the liquid solution. Values have been optimized unless a source is listed, in which case the values have been taken from that source

AX	BX	$\Delta g_{AB/XX}^{\circ}$	$\Delta g_{AB/XX}^{1\circ}$	$\Delta g_{AB/XX}^{01}$	Source
NaCl	MgCl <sub>2</sub>	-10 200-1.6 T	660.5	-4650-1.5 T	15
NaCl	PuCl <sub>3</sub>	-8450	-3220	-5658	28
NaCl	NdCl <sub>3</sub>	-5500-8.5 T	-6000 + 6 T	-5500 + 6 T	This work
NaCl	CeCl <sub>3</sub>	-11 200-0.5 T	2000-4 T	-4000 + 2 T	This work
NaCl	UCl <sub>3</sub>	-11 000 + 3.5 T	3000-6 T	-10 000 + 2 T	This work <sup>a</sup>
MgCl <sub>2</sub>	PuCl <sub>3</sub>	2400-0.7 T	0.3 T		This work
MgCl <sub>2</sub>	NdCl <sub>3</sub>	2000-2.8 T	2 T	4.5 T	This work
MgCl <sub>2</sub>	CeCl <sub>3</sub>	2300-1.6 T		2200-0.5 T	This work
MgCl <sub>2</sub>	UCl <sub>3</sub>	2000	2000	3000-0.5 T	This work

<sup>a</sup> Re-optimized from the work of Yingling *et al.*<sup>35</sup> to reproduce the same phase diagram with a different choice of end-member function for UCl<sub>3</sub>



in oxide systems, where  $\text{CeO}_2$  and  $\text{Ce}_2\text{O}_3$  can be used as simulant for  $\text{PuO}_2$  and  $\text{Pu}_2\text{O}_3$ , respectively. In a molten salt environment, Pu is mostly stable in its +3 oxidation state (*i.e.*  $\text{PuCl}_3$ ), but can oxidize to +4 in case oxychlorides or oxides form (*i.e.*  $\text{PuOCl}_2$ ,<sup>42,43</sup>  $\text{PuO}_2$ <sup>44</sup>). Only a few lanthanides are stable in the +4 oxidation state, among which Ce, which is why Ce seems like the most logical choice at first glance. However, when looking at the melting behaviour and ionic radius, it may not be the most suitable lanthanide to fill the role of simulant element, as we show in this work. This observation is in agreement with the work of Goloviznina *et al.*,<sup>45</sup> who show based on DFT calculations and MD simulations that  $\text{NdCl}_3$  is the most appropriate simulant for  $\text{PuCl}_3$  with respect to density and viscosity in molten  $\text{NaCl-MCl}_3$  ( $M = \text{Nd, Ce, Pu}$ ) chlorides.

A comparison of the melting behaviour of different lanthanide chloride-alkali chloride systems has been made by collecting experimental liquidus data reported in the literature for the systems  $\text{NaCl-MCl}_3$ .<sup>8–10,35,40,46–60</sup> The decision on which potential simulants to consider is based on the data shown in Fig. 1, which allows for a pre-selection based on similarity with Pu and U at first glance. Shown in these figures is the melting behaviour of  $\text{NaCl-MCl}_3$  ( $M = \text{La-Yb, Pu, U}$ ) mixtures as a function of  $x(\text{MCl}_3)$ , *i.e.* the molar fraction of the  $\text{MCl}_3$  species. The systems with NaCl were selected because NaCl is part of the base fuel salt, and there is an abundance of data in the literature.

As seen in Fig. 1b, the liquidus line of the  $\text{NaCl-NdCl}_3$  system is almost perfectly overlapping with that of the  $\text{NaCl-PuCl}_3$  system. Following the conclusion of Goloviznina *et al.*<sup>45</sup> that  $\text{NdCl}_3$  is the prime candidate for simulating the density and viscosity of  $\text{PuCl}_3$  in  $\text{NaCl-MCl}_3$  molten chlorides, this work shows that it is also the best simulant with respect to the melting behaviour. Also shown in this figure is the liquidus line of the  $\text{NaCl-CeCl}_3$  system, which has been cited as simulant for Pu and U in the literature,<sup>38–41</sup> but bears the closest resemblance to the liquidus in the  $\text{NaCl-UCl}_3$  system. From

this first analysis, we focused our efforts on the chemistry of the  $\text{NaCl-RECl}_3$  and  $\text{NaCl-MgCl}_2\text{-RECl}_3$  ( $\text{RE} = \text{Ce, Nd}$ ) systems as most suitable surrogates for the corresponding  $\text{AnCl}_3$  ( $\text{An} = \text{U, Pu}$ ) systems. A number of open issues were identified for those systems, which we have explored in detail as described hereafter.

## 3.2 Insights into $\text{NaCl-RECl}_3$ ( $\text{RE} = \text{Ce, Nd}$ ) chemistry

### 3.2.1 $\text{NaCl-NdCl}_3$ .

Experimental data have been reported in the literature on the  $\text{NaCl-NdCl}_3$  system by Seifert *et al.* in 1988,<sup>61</sup> who performed Differential Thermal Analysis (DTA) and XRD analyses. They found by XRD that an intermediate compound exists, which they assigned to  $\text{Na}_3\text{Nd}_5\text{Cl}_{18}$ , also written as  $\text{Na}_{0.67}(\text{Na}_{0.33}\text{Nd}_{1.67})\text{Cl}_6$  (space group  $P6_3/m$ <sup>61</sup>). Sato *et al.*<sup>10</sup> also presented an experimental investigation of this system in 1998 using DTA and XRD, and they retained the intermediate compound found by Seifert *et al.*,  $\text{Na}_3\text{Nd}_5\text{Cl}_{18}$  in their assessment. They suggested that a homogeneity range exists at elevated temperatures, specifically between  $x(\text{NdCl}_3) = 0.59$  and  $x(\text{NdCl}_3) = 0.70$  and  $T = (573\text{--}873)$  K. According to the sketched phase diagram Sato *et al.* reported, the homogeneity range is only stable at elevated temperatures, while the room temperature composition remains  $\text{Na}_3\text{Nd}_5\text{Cl}_{18}$ . However, neither Sato *et al.* nor Seifert *et al.* reported detailed crystallographic information on the intermediate compound, notably the atomic positions in the crystal structure. Earlier DTA assessments by Igarashi *et al.* (1990)<sup>9</sup> and Sharma *et al.* (1992)<sup>8</sup> agreed about the existence of an intermediate, but suggested the intermediate  $\text{NaNd}_3\text{Cl}_{10}$  instead, and indicated no homogeneity range. In view of the discrepancies between the literature studies, new investigations of the crystal structures of this compound were performed in this work to address the remaining questions.

In addition to the phase diagram studies found in the literature, single-crystal studies of the intermediate compound by Lissner *et al.* (1994)<sup>12</sup> dived more in detail into the crystal

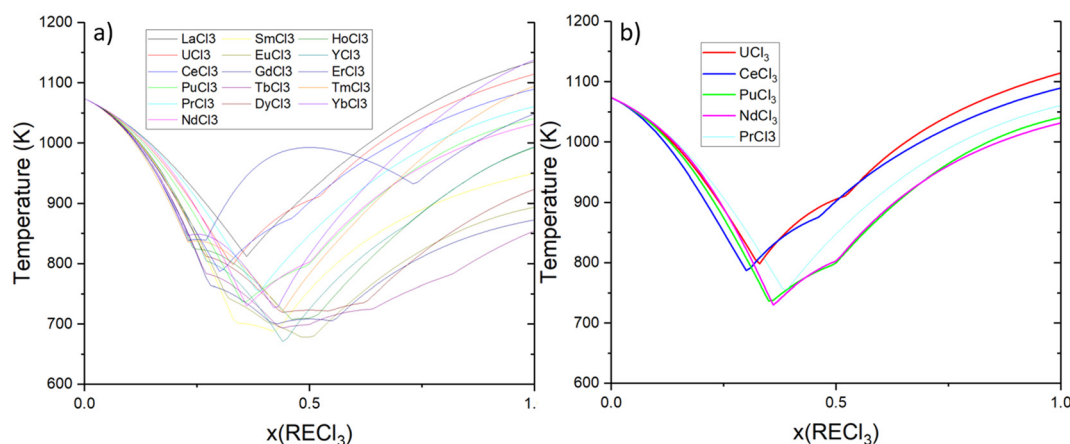


Fig. 1 Liquidus lines of  $\text{NaCl-MCl}_3$  systems ( $M = \text{La-Yb, Y, U, Pu}$ ) reported in the literature<sup>8–10,35,40,46–60</sup> (a), and selected liquidus lines for potential simulant systems (b).



structure chemistry. They reported a structure of  $\text{Na}_{0.698}(\text{Na}_{0.35}\text{Ce}_{1.65})\text{Cl}_6$ , corresponding to a general stoichiometry of  $\text{Na}_x(\text{Na}_{\frac{x}{2}}\text{Nd}_{1-\frac{x}{2}})\text{Cl}_3$  (space group  $P6_3/m$ ). The existence of this compound is confirmed in our work with new experimental investigations, and the description of Lissner *et al.* is thus retained. Moreover, the extent of the homogeneity range is scrutinized in detail for the first time. While the  $\text{Na}_x(\text{Na}_{\frac{x}{2}}\text{Nd}_{1-\frac{x}{2}})\text{Cl}_3$  notation gives an insight into the crystallography (e.g. the shared Na/Nd position), in this work we will use the simpler notation  $\text{Na}_{3x}\text{Nd}_{2-x}\text{Cl}_6$  or  $\text{Na}_{2x}(\text{Na}_x\text{Nd}_{2-x})\text{Cl}_6$ . Based on the atomic positions Lissner *et al.* reported for a sample of stoichiometry  $\text{Na}_{0.608}(\text{Na}_{0.304}\text{Nd}_{1.696})\text{Cl}_6$ , we can define a general description for the  $\text{Na}_{3x}\text{Nd}_{2-x}\text{Cl}_6$  phase that has been used in this work (see Table 7, Fig. 2).

Several samples were prepared in this work with varying (NaCl :  $\text{NdCl}_3$ ) ratios as detailed in Section 2.1.1, with the aim of confirming the crystal structure model, and defining the limits of the homogeneity range. Mixtures were prepared within the expected homogeneity range, as well as in the two-phase domains. The mixtures were subjected to thermal treatment at  $T = 693$  K for at least 48 hours. A few quenching experiments were also performed at compositions  $x(\text{NdCl}_3) = 0.60, 0.625$  and  $0.65$  at  $T = 773$  K. The aim of these experiments was to investigate the behaviour of this compound both at elevated temperatures and at room temperature, following the hints in the literature by Sato *et al.*<sup>10</sup> and Lissner *et al.*<sup>12</sup>

Shown in Fig. 4 is the profile refinement of the composition  $x(\text{NdCl}_3) = 0.65$ , collected at room temperature using sXRD. This refinement shows that a single phase exists at this composition, with no detectable amounts of the end members NaCl and  $\text{NdCl}_3$ . The same was observed for the compositions  $x(\text{NdCl}_3) = 0.55, 0.6$  and  $0.625$  in the same binary system, confirming the existence of an intermediate with a considerable homogeneity range. The  $\text{Na}_{3x}\text{Nd}_{2-x}\text{Cl}_6$  phase adopts the same crystal structure symmetry as  $\text{NdCl}_3$  (also hexagonal, in space group  $P6_3/m$ <sup>13</sup>). Upon addition of sodium to the  $\text{NdCl}_3$  structure, partial substitution of sodium on the Nd site ( $2c$ ) occurs, while the rest of the sodium is located on the  $(0,0,0)$  position ( $2b$ ) with an occupancy

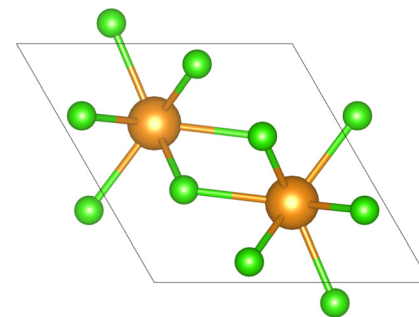


Fig. 3 Crystal structure of  $\text{NdCl}_3$  as reported by Meyer *et al.*<sup>13</sup> viewed along the  $c$ -axis, with the elements Nd and Cl indicated in orange and green respectively.

equal to  $x$ . The shared Nd/Na2 site is nine-fold coordinated (same as in the  $\text{NdCl}_3$ ), while the Na1 site is six-fold coordinated. The crystal structures of  $\text{Na}_{3x}\text{Nd}_{2-x}\text{Cl}_6$  and  $\text{NdCl}_3$  are shown in Fig. 2 and 3, respectively to illustrate this. The atomic positions obtained from the refinements of the intermediates  $\text{Na}_{3x}\text{RE}_{2-x}\text{Cl}_6$  are presented in Table 7.

At composition  $x(\text{NdCl}_3) = 0.70$ , as shown in Fig. 5, the first traces of the end member  $\text{NdCl}_3$  become apparent, showing that the limiting composition of the homogeneity range lies between  $x(\text{NdCl}_3) = 0.65$  and  $x(\text{NdCl}_3) = 0.70$ . Similarly, the other limiting composition, *i.e.* that on the NaCl-rich side, was found between  $x(\text{NdCl}_3) = 0.50$  and  $x(\text{NdCl}_3) = 0.55$ . Contrary to the assessments of Seifert *et al.*<sup>11</sup> and Sato *et al.*,<sup>10</sup> the solid solution in this system was observed to be stable at room temperature, rather than exclusively at elevated temperatures.

The stability of the solid solution at elevated temperatures was moreover investigated through quenching experiments, where three samples at compositions  $x(\text{NdCl}_3) = 0.6, 0.625$  and  $0.65$  were heated up to 773 K and subsequently quenched in a water bath to preserve the crystal structures stable at high temperatures. These experiments showed that at  $T = 773$  K, the crystal structure was still that of the single-phase solid solution. Furthermore, to rule out kinetic effects that limit the formation of the solid solution, we performed a synthesis experiment at  $x(\text{NdCl}_3) = 0.75$  with two different heating durations (48 h and 96 h). No appreciable difference was observed between the two experiments, thus we conclude that 48 h is enough time for the synthesis experiment to reach thermodynamic equilibrium.

The progression of the cell volume of the intermediate compound  $\text{Na}_{3x}\text{Nd}_{2-x}\text{Cl}_6$  is shown in Fig. 7 as a function of composition, and the values are reported in Table 6. On the left side of the single-phase region (*i.e.* from  $x(\text{NdCl}_3) = 0.55$ – $0.65$ ), a mixture of NaCl and  $\text{Na}_{3x}\text{Nd}_{2-x}\text{Cl}_6$  is found, and the solid solution reaches the volume at its limiting composition. On the right side of the solubility range, a mixture of  $\text{NdCl}_3$  and  $\text{Na}_{3x}\text{Nd}_{2-x}\text{Cl}_6$  is found, but the size of the unit cell of the intermediate keeps shrinking as the  $\text{NdCl}_3$  fraction increases. We would expect the volume of the intermediate compound to remain constant and equal to that at the limiting composition of the homogeneity range instead. The reason for this is as of yet

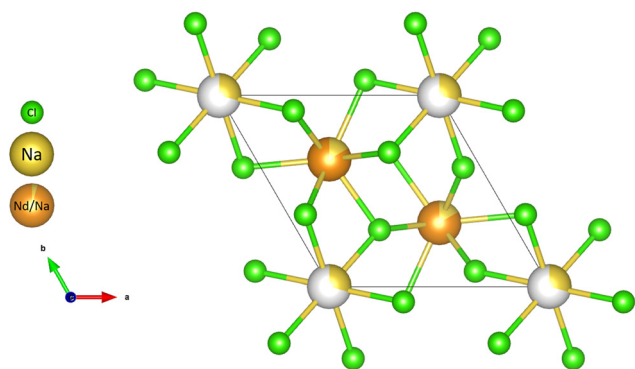


Fig. 2 Crystal structure of the  $\text{Na}_{0.335}(\text{Na}_{0.168}\text{Nd}_{1.832})\text{Cl}_6$  compound obtained in this work viewed along the  $c$ -axis, with the elements Na, Nd and Cl indicated in yellow, orange and green respectively. The corresponding atomic parameters are listed in Table 7.



not known, and should be subjected to further investigation. As shown before in Fig. 4 and 5, several samples in the NaCl–NdCl<sub>3</sub> system were measured with synchrotron-XRD ( $\lambda = 0.7653 \text{ \AA}$ ), labelled (sXRD) in Fig. 7, while others were measured by conventional laboratory XRD. The aim of the synchrotron experiments was to investigate the possible presence of end-members

towards the limiting compositions, *i.e.*  $x(\text{NdCl}_3) = 0.55$  and  $0.7$ , given the higher resolution of s-XRD compared to lab-XRD, as well as obtain a high-resolution XRD of the single-phase Na<sub>3x</sub>Nd<sub>2-x</sub>Cl<sub>6</sub>. The results of the synchrotron-XRD are very similar to the measurements carried out using lab XRD, confirming the reliability of the results.

The phase diagram has then been optimized based on the experimental DTA data from Sato *et al.*,<sup>10</sup> shown in solid black circles in Fig. 6. The data from Sato *et al.* largely agree with the work of Seifert *et al.*,<sup>61</sup> with the exception of the peritectic equilibrium. Seifert *et al.* measured two sub-liquidus equilibria between  $x(\text{NdCl}_3) = 0.5$  and  $x(\text{NdCl}_3) = 0.95$ , whereas Sato *et al.* only measured one. This single peritectic equilibrium was also reported by Igarashi *et al.*<sup>9</sup> and Sharma *et al.*<sup>8</sup> Moreover, the work of Sharma *et al.* and Igarashi *et al.* reported the eutectic equilibrium up to  $x(\text{NdCl}_3) = 0.8$ , while Sato *et al.* and Seifert *et al.* reported the eutectic up to  $x(\text{NdCl}_3) = 0.5$  and  $0.6$ , respectively. A possible explanation for the fact that Sharma *et al.* and Igarashi *et al.* measured the eutectic equilibrium up to higher NdCl<sub>3</sub> content could be a contamination (Sharma *et al.* report a minor NdOCl contamination), or a sub-cooling effect (Igarashi *et al.* analysed the measured cooling curves). Another explanation could be that the kinetics of formation of the solid solution is slow, meaning that if previous authors measured with high heating rates, they could potentially observe metastable phases in the system.

Additionally, the limits of the homogeneity range and the stability at room temperature of the intermediate Na<sub>3x</sub>Nd<sub>2-x</sub>Cl<sub>6</sub> have been included in the optimisation using the experimental

**Table 6** Refined lattice parameters of the Na<sub>3x</sub>RE<sub>2-x</sub>Cl<sub>6</sub> phase in all investigated samples in the NaCl–RECl<sub>3</sub> (RE = Nd, Ce) systems, also shown in Fig. 7

$x(\text{RECl}_3)$	$a, b$ (Å)	$c$ (Å)	Volume (Å <sup>3</sup> )	Method
<b>NaCl–NdCl<sub>3</sub></b>				
0.500 <sup>a</sup>	7.5343(4)	4.2326(5)	208.1(3)	XRD
0.548 <sup>b</sup>	7.5340(5)	4.2321(3)	208.0(2)	XRD
0.548 <sup>b</sup>	7.5345(4)	4.2322(5)	208.1(3)	sXRD
0.600 <sup>b</sup>	7.5385(6)	4.2294(3)	208.0(3)	XRD
0.625 <sup>b</sup>	7.5279(3)	4.2307(3)	207.6(2)	XRD
0.625 <sup>b</sup>	7.5269(4)	4.2310(5)	207.6(3)	sXRD
0.650 <sup>b</sup>	7.5210(3)	4.2300(3)	207.2(2)	XRD
0.700 <sup>c</sup>	7.5130(5)	4.2304(5)	206.8(3)	XRD
0.700 <sup>c</sup>	7.5134(4)	4.2293(5)	206.8(2)	sXRD
0.750 <sup>c</sup>	7.5069(4)	4.2291(5)	206.4(3)	XRD
<b>NaCl–CeCl<sub>3</sub></b>				
0.500 <sup>a</sup>	7.5596(4)	4.3070(4)	213.2(2)	XRD
0.543 <sup>a</sup>	7.5593(4)	4.3082(4)	213.2(2)	XRD
0.588 <sup>b</sup>	7.5584(2)	4.3078(2)	213.1(1)	XRD
0.630 <sup>b</sup>	7.5550(5)	4.3057(4)	212.8(2)	XRD
0.649 <sup>b</sup>	7.5513(8)	4.3078(7)	212.7(4)	XRD
0.700 <sup>c</sup>	7.5470(4)	4.3052(4)	212.4(2)	XRD
0.750 <sup>c</sup>	7.5392(6)	4.3056(8)	211.9(3)	XRD

<sup>a</sup> {NaCl + Na<sub>3x</sub>RE<sub>2-x</sub>Cl<sub>6</sub>}. <sup>b</sup> Single phase Na<sub>3x</sub>RE<sub>2-x</sub>Cl<sub>6</sub>. <sup>c</sup> {RECl<sub>3</sub> + Na<sub>3x</sub>RE<sub>2-x</sub>Cl<sub>6</sub>}.

**Table 7** Crystallographic data of the Na<sub>3x</sub>RE<sub>2-x</sub>Cl<sub>6</sub> solid solution (SGR P6<sub>3</sub>/m; RE = Ce, Nd) obtained from the refinements of the XRD data in this work. Compositions at which sXRD data was used are marked with an asterisk. The occupancy is treated as variable in this work, and is based on molar fraction of RECl<sub>3</sub> in the solid solution:  $x = \frac{1 - x(\text{RECl}_3)}{x(\text{RECl}_3) + \frac{1}{2}}$ . Marked in bold are the compositions at which only single-phase Na<sub>3x</sub>RE<sub>2-x</sub>Cl<sub>6</sub> was found

$x(\text{RECl}_3)$	Intermediate stoichiometry	Site	Element	Wyckoff position	X	Y	Z	Occupancy
All	—	Na1	Na	2b	0	0	0	$x$
All	—	RE1	RE	2c	$\frac{1}{3}$	$\frac{2}{3}$	$\frac{1}{4}$	$1 - \frac{x}{2}$
All	—	Na2	Na	2c	$\frac{2}{3}$	$\frac{1}{3}$	$\frac{1}{4}$	$\frac{x}{2}$
<b>RE = Nd</b>								
0.500	Na <sub>0.429</sub> (Na <sub>0.214</sub> Nd <sub>1.786</sub> )Cl <sub>6</sub>	Cl1	Cl	6h	0.3816(6)	0.2967(6)	$\frac{1}{4}$	1
0.548	Na <sub>0.429</sub> (Na <sub>0.214</sub> Nd <sub>1.786</sub> )Cl <sub>6</sub>				0.3760(6)	0.2926(6)		
0.548*	Na <sub>0.429</sub> (Na <sub>0.214</sub> Nd <sub>1.786</sub> )Cl <sub>6</sub>				0.3872(1)	0.3027(1)		
0.600	Na <sub>0.364</sub> (Na <sub>0.182</sub> Nd <sub>1.818</sub> )Cl <sub>6</sub>				0.3783(8)	0.2937(9)		
0.623	Na <sub>0.335</sub> (Na <sub>0.168</sub> Nd <sub>1.832</sub> )Cl <sub>6</sub>				0.3826(6)	0.2986(7)		
0.623*	Na <sub>0.335</sub> (Na <sub>0.168</sub> Nd <sub>1.832</sub> )Cl <sub>6</sub>				0.3902(2)	0.3032(2)		
0.650	Na <sub>0.304</sub> (Na <sub>0.152</sub> Nd <sub>1.848</sub> )Cl <sub>6</sub>				0.3736(7)	0.2938(7)		
0.700	Na <sub>0.304</sub> (Na <sub>0.152</sub> Nd <sub>1.848</sub> )Cl <sub>6</sub>				0.3915(2)	0.3049(2)		
0.700*	Na <sub>0.304</sub> (Na <sub>0.152</sub> Nd <sub>1.848</sub> )Cl <sub>6</sub>				0.3763(6)	0.2918(2)		
0.750	Na <sub>0.304</sub> (Na <sub>0.152</sub> Nd <sub>0.848</sub> )Cl <sub>6</sub>				0.3752(7)	0.2903(7)		
<b>RE = Ce</b>								
0.500	Na <sub>0.379</sub> (Na <sub>0.190</sub> Ce <sub>1.810</sub> )Cl <sub>6</sub>	Cl1	Cl	6h	0.3758(6)	0.2948(6)	$\frac{1}{4}$	1
0.543	Na <sub>0.379</sub> (Na <sub>0.190</sub> Ce <sub>1.810</sub> )Cl <sub>6</sub>				0.3754(6)	0.2920(6)		
0.588	Na <sub>0.379</sub> (Na <sub>0.190</sub> Ce <sub>1.810</sub> )Cl <sub>6</sub>				0.3736(5)	0.2914(5)		
0.630	Na <sub>0.328</sub> (Na <sub>0.164</sub> Ce <sub>1.834</sub> )Cl <sub>6</sub>				0.3737(4)	0.2908(4)		
0.649	Na <sub>0.305</sub> (Na <sub>0.153</sub> Ce <sub>1.847</sub> )Cl <sub>6</sub>				0.3768(6)	0.2942(6)		
0.703	Na <sub>0.305</sub> (Na <sub>0.153</sub> Ce <sub>1.847</sub> )Cl <sub>6</sub>				0.3804(6)	0.2974(7)		
0.750	Na <sub>0.305</sub> (Na <sub>0.153</sub> Ce <sub>1.847</sub> )Cl <sub>6</sub>				0.3732(6)	0.2913(6)		



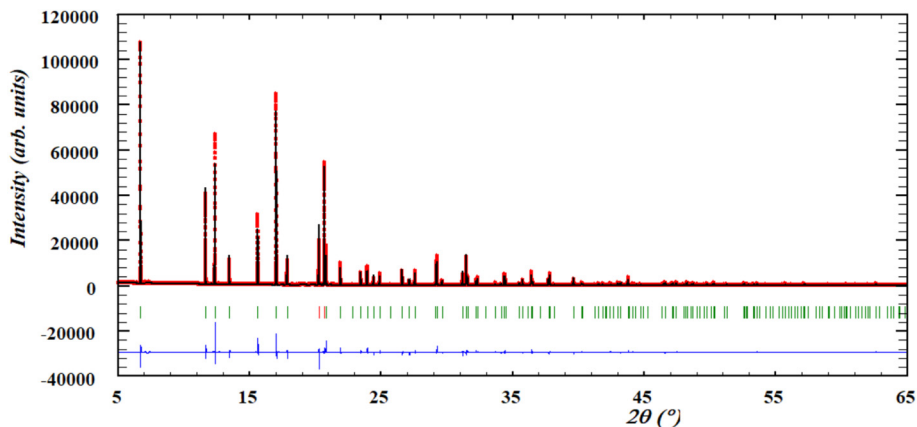


Fig. 4 Profile refinement of the sXRD ( $\lambda = 0.7653 \text{ \AA}$ ) at  $x(\text{NdCl}_3) = 0.623$  in the NaCl–NdCl<sub>3</sub> system, showing the single phase Na<sub>0.335</sub>(Na<sub>0.168</sub>Nd<sub>1.832</sub>)Cl<sub>6</sub>. The observed intensity (red circles) is shown alongside the calculated intensity (black line), and the difference between the two is shown (blue line). The angles at which reflections occur, *i.e.* the Bragg positions, are shown as well (green, vertical lines).

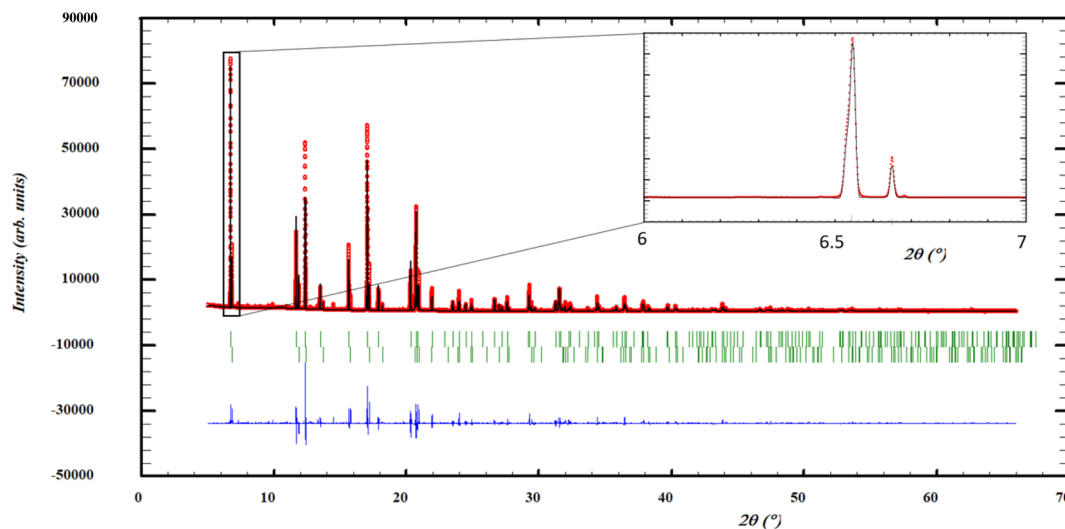


Fig. 5 Profile refinement of the sXRD ( $\lambda = 0.7653 \text{ \AA}$ ) at  $x(\text{NdCl}_3) = 0.70$  in the NaCl–NdCl<sub>3</sub> system, with phases Na<sub>0.304</sub>(Na<sub>0.152</sub>Nd<sub>1.848</sub>)Cl<sub>6</sub> and NdCl<sub>3</sub><sup>13</sup> included in the refinement. The zoomed part of the figure shows the distinct separation of the Na<sub>3</sub>xNd<sub>2-x</sub>Cl<sub>6</sub> peak (left) and the NdCl<sub>3</sub> peak (right). The observed intensity (red circles) is shown alongside the calculated intensity (black line), and the difference between the two is shown (blue line). The angles at which reflections occur, *i.e.* the Bragg positions, are shown as well (green, vertical lines).

data obtained in this work. The mixing enthalpy of this system has been measured by Gaune-Escard *et al.*<sup>62</sup> at  $T = 1124 \text{ K}$  and has been optimized based on these experimental data. The calculated mixing enthalpy of this system is presented in Fig. 9. The intermediate compound Na<sub>3</sub>xNd<sub>2-x</sub>Cl<sub>6</sub> has been included in the thermodynamic model as a solid solution with NaCl and NaNd<sub>2</sub>Cl<sub>7</sub> (corresponding to Na<sub>0.571</sub>(Na<sub>0.286</sub>Nd<sub>1.714</sub>)Cl<sub>6</sub> at  $x(\text{NdCl}_3) = 0.66$ ) as end-members to account for the limiting compositions of the solubility range.

**3.2.2 NaCl–CeCl<sub>3</sub>.** Similarly, the salt system NaCl–CeCl<sub>3</sub> has been investigated experimentally by various authors in the literature. Most authors have interpreted the system as a simple binary eutectic system,<sup>63–66</sup> with Storonkin *et al.*<sup>67</sup> suggesting solubility of NaCl in a hypothetical low-temperature polymorphic phase of CeCl<sub>3</sub>. Since CeCl<sub>3</sub> does not have a low-

temperature phase, that interpretation is discarded. Krämer and Meyer (1990)<sup>68</sup> and Lissner *et al.* (1992)<sup>12</sup> reported single-crystal studies of Na<sub>0.76</sub>(Na<sub>0.38</sub>Ce<sub>1.62</sub>)Cl<sub>6</sub> and Na<sub>0.698</sub>(Na<sub>0.35</sub>Ce<sub>1.65</sub>)Cl<sub>6</sub>, respectively, again corresponding to a general stoichiometry of Na<sub>3</sub>xCe<sub>2-x</sub>Cl<sub>6</sub> (space group  $P6_3/m$ ). Seifert *et al.*<sup>11</sup> suggested, based on DTA and XRD, that a solid solution between CeCl<sub>3</sub> and an intermediate compound of composition Na<sub>3</sub>Ce<sub>5</sub>Cl<sub>18</sub> existed.

In addition to the data found in the literature, an experimental investigation of the intermediate compound Na<sub>3</sub>xCe<sub>2-x</sub>Cl<sub>6</sub> was performed, like in the NaCl–NdCl<sub>3</sub> system, mostly to gain further insight into the composition of the intermediate and possible existence of a homogeneity range. Synthesis experiments at several compositions were performed to identify the solubility limits of this intermediate compound.



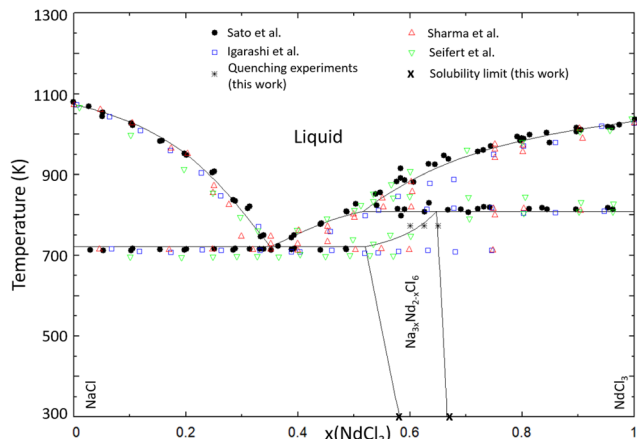


**Fig. 6** Phase diagram of the NaCl–NdCl<sub>3</sub> system calculated with the thermodynamic model presented in this work. Experimental data from Sato *et al.*<sup>10</sup> (closed black circles), Igarashi *et al.*<sup>9</sup> (open blue squares), Sharma *et al.*<sup>8</sup> (open upward green triangles) and Seifert *et al.*<sup>61</sup> (open downward red triangles).

A single-phase intermediate compound was found at compositions  $x(\text{CeCl}_3) = 0.60, 0.625$  and  $0.65$ , while NaCl was observed at compositions  $x(\text{CeCl}_3) \leq 0.55$  and CeCl<sub>3</sub> was observed at compositions  $x(\text{CeCl}_3) \geq 0.70$ . Based on these results, we conclude that the limiting concentrations of this solid solution are between  $x(\text{CeCl}_3) = 0.55$  and  $0.60$  on the NaCl-rich side, and  $x(\text{CeCl}_3) = 0.65$  and  $0.70$  on the CeCl<sub>3</sub>-rich side. The progression of the cell volume of the intermediate compound Na<sub>3x</sub>Ce<sub>2-x</sub>Cl<sub>6</sub>, obtained from the refinements performed in this work, is shown in Fig. 7 and reported in Table 6. The compositions at which a single phase solid solution is observed obey the expected linear trend. Furthermore, like in the Na<sub>3x</sub>Nd<sub>2-x</sub>Cl<sub>6</sub> intermediate, the limiting composition on the left side of the solubility range shows that the cell volume reaches a maximum at compositions  $x(\text{CeCl}_3) \leq$

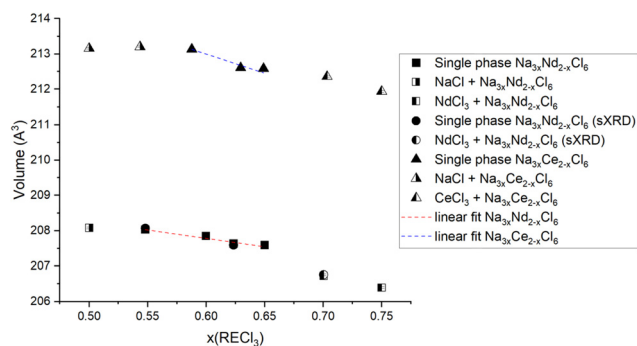


**Fig. 7** Cell volumes calculated from the profile refinements carried out in this work in the NaCl–RECl<sub>3</sub> (RE = Ce, Nd) systems. The data are both from synchrotron XRD and lab XRD, and the results obtained with these techniques are in good agreement with each other. A linear trend is visible in the single-phase solid solution following the insertion of the Na cation in the interstitial sites of the Na<sub>3x</sub>RE<sub>2-x</sub>Cl<sub>6</sub> crystal structure. The refined values are also given in Table 6.

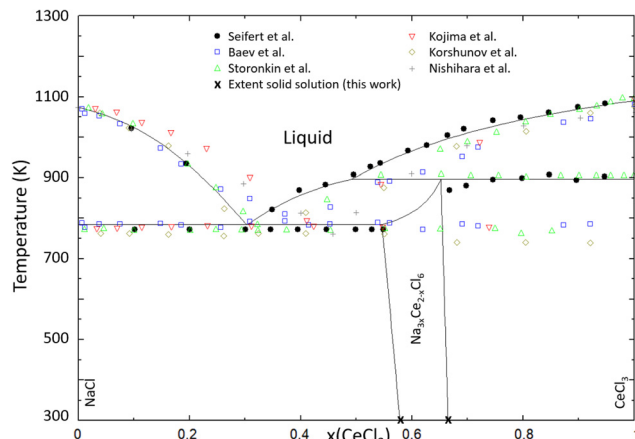


**Fig. 8** Phase diagram of the NaCl–CeCl<sub>3</sub> system calculated with the thermodynamic model presented in this work. Experimental data from Seifert *et al.*<sup>11</sup> (closed black circles), Baev *et al.*<sup>63</sup> (open blue squares), Storonkin *et al.*<sup>70</sup> (open upward green triangles), Kojima *et al.*<sup>66</sup> (open downward red triangles), Korshunov *et al.*<sup>64</sup> (open gold diamonds) and Nishihara *et al.*<sup>65</sup> (grey pluses).

0.59. The same trend in the cell volume decreasing beyond the solubility limit of the rare earth chloride (that was also seen in the NaCl–NdCl<sub>3</sub> system), is observed here.

The NaCl–CeCl<sub>3</sub> thermodynamic model was optimized based on the DTA data from Seifert *et al.*<sup>11</sup> The measurement of the eutectic equilibrium past  $x(\text{CeCl}_3) = 0.55$  in the other sources could be due to contaminations. Kojima *et al.*<sup>66</sup> and Nishihara *et al.*<sup>65</sup> report CeCl<sub>3</sub> purities  $\leq 98\%$ , and Storonkin *et al.*<sup>67</sup> measured what they interpret as a polymorphic transition in CeCl<sub>3</sub>, which is an indication that they also had impurities in their CeCl<sub>3</sub> batch. Baev *et al.*<sup>63</sup> and Korshunov *et al.*<sup>64</sup> do not specify their measurement method or end-member purity, so it is difficult to say what could have gone wrong.

The extent and stability of the intermediate compound Na<sub>3x</sub>Ce<sub>2-x</sub>Cl<sub>6</sub> along with its solubility range was optimized based on the experimental data obtained in this work. The phase diagram of this system is presented in Fig. 8. The mixing enthalpy of this system was optimized based on the experimental data from Papatheodorou *et al.*<sup>69</sup> and is shown in Fig. 9. Like in the NaCl–NdCl<sub>3</sub> system, the intermediate compound Na<sub>3x</sub>Ce<sub>2-x</sub>Cl<sub>6</sub> has been included in the thermodynamic model as a solid solution between NaCl and NaCe<sub>2</sub>Cl<sub>7</sub> end-members, with again an arbitrary destabilization term of the NaCl end-member of  $+5000 \text{ J mol}^{-1}$ .

**3.2.3 Simulant chemistry in NaCl–MCl<sub>3</sub> systems.** Before an assessment of the simulant representativeness can be made, the melting behaviour of the systems NaCl–UCl<sub>3</sub> and NaCl–PuCl<sub>3</sub> must be addressed. The system NaCl–UCl<sub>3</sub> has been investigated experimentally by Kraus *et al.*<sup>71</sup> Sooby *et al.*<sup>40</sup> and Yingling *et al.*<sup>35</sup> The former reported the use of thermal analysis to obtain their results without further specifying their measurement method, whereas Sooby *et al.* and Yingling *et al.* used DSC. Both Kraus *et al.* and Sooby *et al.* interpret this system as a simple binary eutectic system. Yingling *et al.*,



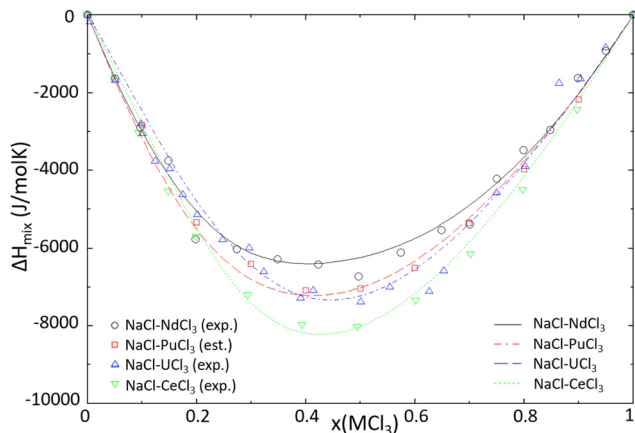


**Fig. 9** Calculated mixing enthalpies of the NaCl–MCl<sub>3</sub> (M = Ce, Nd, U, Pu) systems at  $T = 1125$  K using the thermodynamic model presented in this work (NaCl–NdCl<sub>3</sub> and NaCl–CeCl<sub>3</sub>), by Yingling *et al.*<sup>35</sup> (NaCl–UCl<sub>3</sub>) and by Dumaire *et al.*<sup>28</sup> (NaCl–PuCl<sub>3</sub>). Experimental data from Gaune-Escard *et al.*<sup>62</sup> (NaCl–NdCl<sub>3</sub>, open black circles) at  $T = 1124$  K, Papatheodorou *et al.*<sup>69</sup> (NaCl–CeCl<sub>3</sub>, open downward green triangles) at  $T = 1118$  K and Matsuura *et al.*<sup>72</sup> (NaCl–UCl<sub>3</sub>, open blue upward triangles) at  $T = 1113$  K. Data of the NaCl–PuCl<sub>3</sub> system (open red squares) were estimated using the method of Davis and Rice.<sup>14</sup>

however, suggest that an intermediate compound with the composition NaU<sub>2</sub>Cl<sub>7</sub> (or Na<sub>3</sub>U<sub>5</sub>Cl<sub>18</sub>) exists at elevated temperatures, based on their XRD measurements. Yingling *et al.* fit their thermodynamic model to the liquidus and eutectic equilibria of Kraus *et al.* and Sooby *et al.*, rather than those they measured themselves. Given the results obtained in this work in the NdCl<sub>3</sub> and CeCl<sub>3</sub> systems, we hypothesize that a similar homogeneity range could exist (*i.e.* Na<sub>3x</sub>U<sub>2-x</sub>Cl<sub>6</sub>), although it might be stable only at high temperatures to match with the DSC data. Complementary studies are needed to verify this hypothesis. In this work, the assessment of Yingling *et al.* is largely retained, with a slight re-optimization to account for a difference in the end-members thermodynamic functions: Yingling *et al.* use both UCl<sub>3</sub> and U<sub>2</sub>Cl<sub>6</sub> as end-members, which is not the case in this work.

The available experimental data for the NaCl–PuCl<sub>3</sub> system is much less abundant than for the other NaCl–MCl<sub>3</sub> systems (M = Ce, Nd, U). Bjorklund *et al.*<sup>53</sup> used a combination of thermal analysis (TA) and DTA to investigate the system, and concluded that it is a simple binary eutectic system with no intermediates or solid solubility. Dumaire *et al.*<sup>28</sup> presented a thermodynamic assessment of this system using the same formalism as used in this work. Their assessment of this binary system is therefore retained here as well. However, given the similarities between the NdCl<sub>3</sub> and PuCl<sub>3</sub> systems, the existence of a similar intermediate (Na<sub>3x</sub>Pu<sub>2-x</sub>Cl<sub>6</sub>) needs to be explored by dedicated experiments.

The representativeness of the selected simulants in the NaCl–MCl<sub>3</sub> systems is shown in Fig. 10. In section 4.2, this study will be expanded by adding the comparison with the MgCl<sub>2</sub>–MCl<sub>3</sub> (M = Ce, Nd, U, Pu) systems. Fig. 10 shows that the liquidus of the NaCl–PuCl<sub>3</sub> system is very close to that of

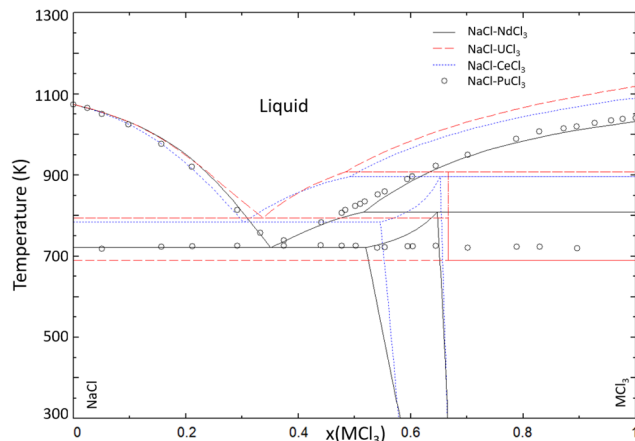


**Fig. 10** Calculated phase diagrams of the systems NaCl–NdCl<sub>3</sub> (solid black line) and NaCl–CeCl<sub>3</sub> (dashed blue line), for which the thermodynamic models were developed in this work, and NaCl–UCl<sub>3</sub> (dashed red line) using the thermodynamic model of Yingling *et al.*<sup>35</sup> slightly altered to account for the different end-members. The models are compared to the experimental data on the NaCl–PuCl<sub>3</sub> system (open black circles) presented by Bjorklund *et al.*<sup>53</sup>

**Table 8** Eutectic equilibria in the NaCl–MCl<sub>3</sub> (M = Ce, Nd, U, Pu) systems as calculated with the thermodynamic models presented in this chapter

System	$x_1$	$T_1$ (K)	Source
PuCl <sub>3</sub>	0.385	725	Dumaire <i>et al.</i> <sup>28</sup>
NdCl <sub>3</sub>	0.355	718	This work
CeCl <sub>3</sub>	0.303	778	This work
UCl <sub>3</sub>	0.337	794	This work

the NaCl–NdCl<sub>3</sub> system. The systems NaCl–CeCl<sub>3</sub> and NaCl–UCl<sub>3</sub> show a similar slope of the liquidus to the PuCl<sub>3</sub> and NdCl<sub>3</sub> systems, but the difference in melting point between these simulants and PuCl<sub>3</sub> leads to a significant deviation of the melting temperature. The observed eutectic composition is similar for all four systems, as shown in Table 8. The eutectic composition and temperature of the NaCl–NdCl<sub>3</sub> system is closest to that of the NaCl–PuCl<sub>3</sub> system, though the latter can be once more explained by the aforementioned difference in melting point of the end-members.

## 4 Modelling NaCl–MgCl<sub>2</sub>–MCl<sub>3</sub> (M = Ce, Nd, U, Pu) systems

### 4.1 Binary systems

As mentioned previously, the thermodynamic model of the NaCl–MgCl<sub>2</sub> system was taken from a previous work.<sup>18</sup> The thermodynamic models of the systems MgCl<sub>2</sub>–MCl<sub>3</sub> (M = Ce, Nd, U, Pu) are presented in this section, and were optimized based on the available data in the literature.

All systems MgCl<sub>2</sub>–MCl<sub>3</sub> (M = Ce, Nd, U, Pu) modelled in this section are simple binary eutectic systems, with no



reported intermediates or solid solubility. The  $\text{MgCl}_2\text{-NdCl}_3$  system has been investigated experimentally by Vogel *et al.*<sup>73</sup> using DTA. Sun *et al.*<sup>74</sup> measured the  $\text{MgCl}_2\text{-CeCl}_3$  system using thermal analysis, without further specifying their measurement technique. The system  $\text{MgCl}_2\text{-UCl}_3$  has been investigated by Desyatnik *et al.*<sup>75</sup> using differential thermal analysis (DTA), and they did not detect any solid solubility using XRD. Finally, the  $\text{MgCl}_2\text{-PuCl}_3$  system has been modeled based on the experimental investigation by Johnson *et al.*<sup>76</sup> In the absence of experimental mixing enthalpy data for any of the systems, the mixing enthalpy of these systems has been estimated with the method of Davis and Rice.<sup>14</sup>

The systems  $\text{MgCl}_2\text{-UCl}_3$  and  $\text{MgCl}_2\text{-PuCl}_3$  have been modelled previously by Beneš *et al.*<sup>31</sup> and are incorporated in the JRCMSD.<sup>31</sup> In order to have our thermodynamic model agree with the estimated mixing enthalpy data, these systems have been reoptimized in this work. The phase diagrams of the systems  $\text{MgCl}_2\text{-CeCl}_3$ ,  $\text{MgCl}_2\text{-UCl}_3$ ,  $\text{MgCl}_2\text{-NdCl}_3$  and  $\text{MgCl}_2\text{-PuCl}_3$  are presented in Fig. 11, 12, 13 and 14, respectively. The calculated mixing enthalpies of these systems are given in Fig. 15, along with the estimated data using the method of Davis and Rice. The CALPHAD model reproduces the experimental phase diagram data well, as well as the estimated mixing enthalpies for the systems.

#### 4.2 Simulant chemistry in $\text{MgCl}_2\text{-MCl}_3$ systems

With the optimized phase diagrams in Fig. 11–14, we can continue the assessment of the simulant of choice in this work. Fig. 16 shows the comparison between the experimental data for the  $\text{MgCl}_2\text{-PuCl}_3$  system, and the thermodynamic models for the  $\text{MgCl}_2\text{-MCl}_3$  ( $M = \text{Ce, Nd, U}$ ) systems, like in section 3.2.3 for the  $\text{NaCl-MCl}_3$  ( $M = \text{Ce, Nd, U, Pu}$ ) systems. Similar to the aforementioned systems with NaCl, the difference in melting point of the  $\text{MCl}_3$  ( $M = \text{Ce, U}$ ) end-member causes a difference in melting behaviour compared to the  $\text{PuCl}_3$  system on the  $\text{MCl}_3$ -rich side of the phase diagram, which is not the

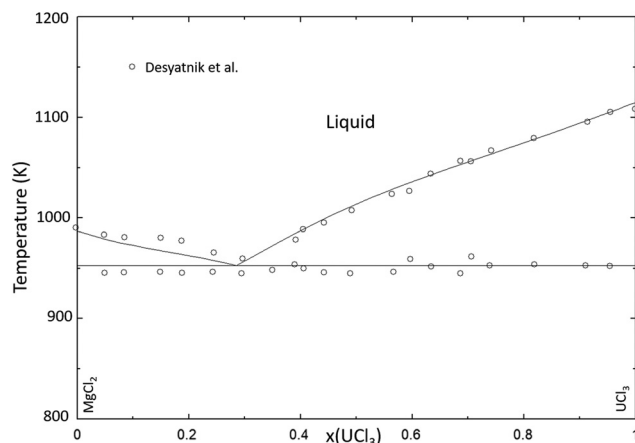


Fig. 12 Phase diagram of the  $\text{MgCl}_2\text{-UCl}_3$  system calculated with the thermodynamic model presented in this work, compared to the experimental data from Desyatnik *et al.*<sup>75</sup>

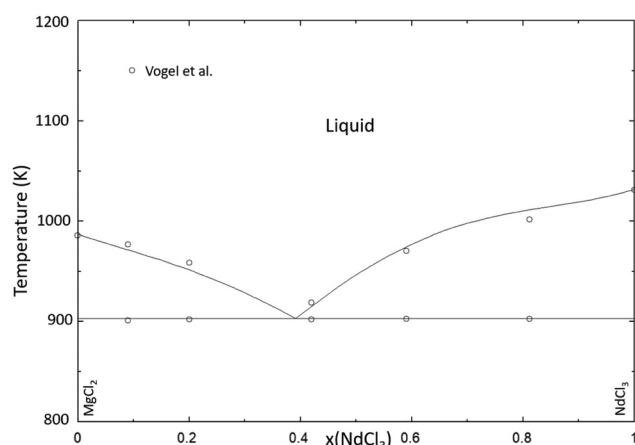


Fig. 13 Phase diagram of the  $\text{MgCl}_2\text{-NdCl}_3$  system, calculated with the thermodynamic model presented in this work and compared to the experimental data from Vogel *et al.*<sup>73</sup>

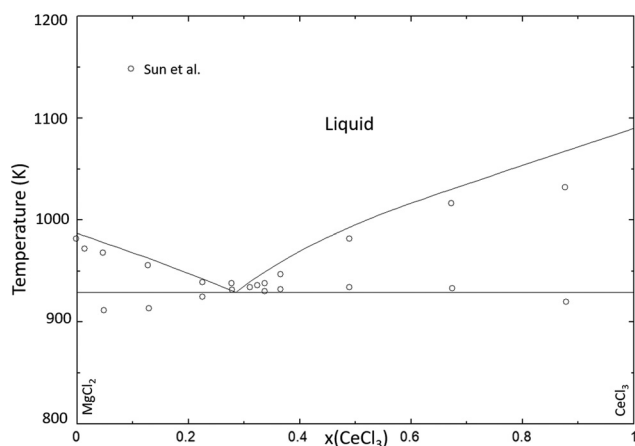


Fig. 11 Phase diagram of the  $\text{MgCl}_2\text{-CeCl}_3$  system, calculated with the thermodynamic model presented in this work and compared to the experimental data from Sun *et al.*<sup>74</sup>

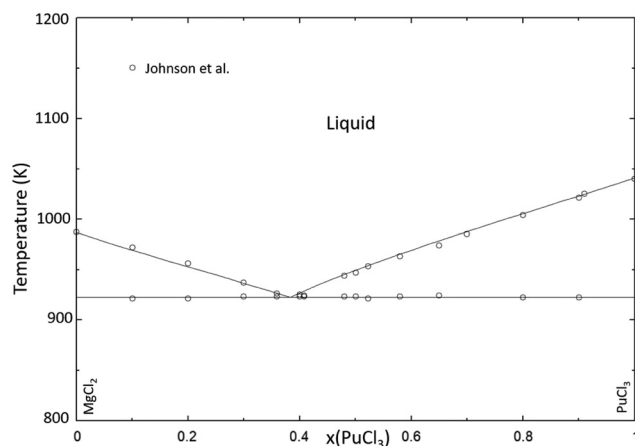


Fig. 14 Phase diagram of the  $\text{MgCl}_2\text{-PuCl}_3$  system calculated with the thermodynamic model presented in this work, compared to the experimental data from Johnson *et al.*<sup>76</sup>



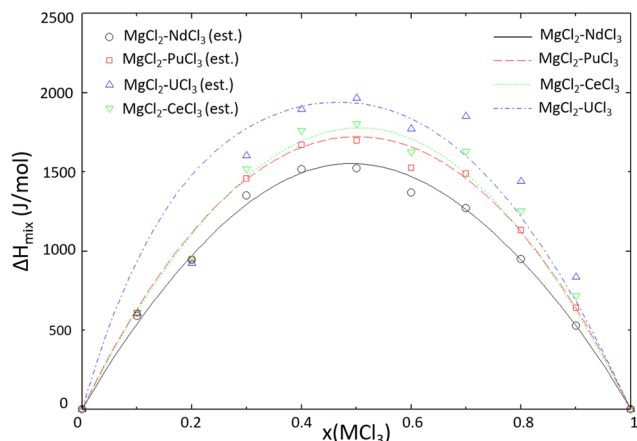


Fig. 15 Mixing enthalpy of the  $\text{MgCl}_2\text{-MCl}_3$  systems ( $M = \text{Ce, Nd, U, Pu}$ ) calculated at  $T = 1123 \text{ K}$ , compared to data estimated using the method of Davis and Rice.<sup>14</sup>

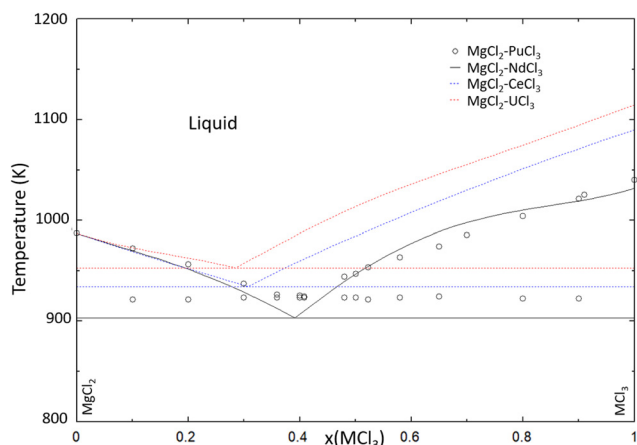


Fig. 16 Calculated phase diagrams of the systems  $\text{MgCl}_2\text{-NdCl}_3$  (solid black line),  $\text{MgCl}_2\text{-CeCl}_3$  (dashed blue line) and  $\text{MgCl}_2\text{-UCl}_3$  (dashed red line) compared to the experimental data on the  $\text{MgCl}_2\text{-PuCl}_3$  system (open black circles) presented by Johnson *et al.*<sup>76</sup>

case for the  $\text{NdCl}_3$  system. The eutectic compositions and temperatures of the  $\text{MgCl}_2\text{-MCl}_3$  systems are given in Table 9. This table shows that while the eutectic temperature of the  $\text{CeCl}_3$  system is marginally closer to that of the  $\text{PuCl}_3$  system, the composition of the  $\text{NdCl}_3$  system is almost identical to that of the  $\text{PuCl}_3$  system.

**Table 9** Eutectic equilibria in the  $\text{MgCl}_2\text{-MCl}_3$  ( $M = \text{Ce, Nd, U, Pu}$ ) systems as calculated with the thermodynamic models presented in this chapter

System	$x_1$	$T_1$ (K)
$\text{PuCl}_3$	0.382	922
$\text{NdCl}_3$	0.383	906
$\text{CeCl}_3$	0.308	934
$\text{UCl}_3$	0.285	953

### 4.3 Ternary systems

From the assessed binary systems, extrapolations to ternary systems  $\text{NaCl-MgCl}_2\text{-MCl}_3$  ( $M = \text{Ce, Nd, U, Pu}$ ) have been made without the addition of ternary excess parameters. This was done because there are no experimental data in the ternary systems available to the best of our knowledge, and to be con-

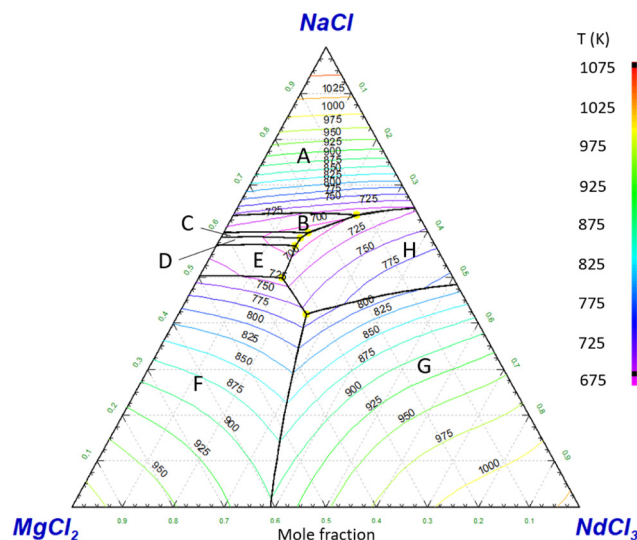


Fig. 17 Projected liquidus surface of the  $\text{NaCl-MgCl}_2\text{-NdCl}_3$  system, calculated with the thermodynamic model presented in this work. Phases A–H listed on the ternary diagram are the primary crystallization phases. Phases listed are  $\text{NaCl}$  (A),  $\text{Na}_6\text{MgCl}_8$  (B),  $\text{Na}_2\text{MgCl}_4$  (C),  $\text{NaMgCl}_3$  (D),  $\text{Na}_2\text{Mg}_3\text{Cl}_8$  (E),  $\text{MgCl}_2$  (F),  $\text{NdCl}_3$  (G) and  $\text{Na}_{3x}\text{Nd}_{2-x}\text{Cl}_6$  (H). The calculated ternary eutectic equilibria are presented in Table 10.

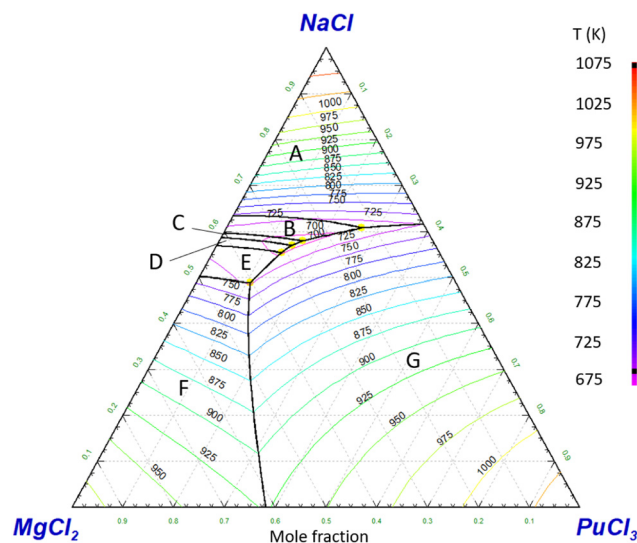


Fig. 18 Projected liquidus surface of the  $\text{NaCl-MgCl}_2\text{-PuCl}_3$  system, calculated with the thermodynamic model presented in this work. Phases A–G listed on the ternary diagram are the primary crystallization phases. Phases listed are  $\text{NaCl}$  (A),  $\text{Na}_6\text{MgCl}_8$  (B),  $\text{Na}_2\text{MgCl}_4$  (C),  $\text{NaMgCl}_3$  (D),  $\text{Na}_2\text{Mg}_3\text{Cl}_8$  (E),  $\text{MgCl}_2$  (F) and  $\text{PuCl}_3$  (G). The calculated ternary eutectic equilibria are presented in Table 10.



**Table 10** Calculated ternary invariant equilibria in the NaCl-MgCl<sub>2</sub>-MCl<sub>3</sub> systems (M = Nd, Pu)

x(NaCl)	x(MgCl <sub>2</sub> )	x(MCl <sub>3</sub> )	T (K)	Invariant equilibrium
<b>NaCl-MgCl<sub>2</sub>-NdCl<sub>3</sub> – This work</b>				
0.419	0.328	0.252	782	MgCl <sub>2</sub> + NdCl <sub>3</sub> + Na <sub>3x</sub> Nd <sub>2-x</sub> Cl <sub>6</sub>
0.499	0.336	0.165	714	MgCl <sub>2</sub> + Na <sub>3x</sub> Nd <sub>2-x</sub> Cl <sub>6</sub> + Na <sub>2</sub> Mg <sub>3</sub> Cl <sub>8</sub>
0.635	0.121	0.244	702	NaCl + Na <sub>6</sub> MgCl <sub>8</sub> + Na <sub>3x</sub> Nd <sub>2-x</sub> Cl <sub>6</sub>
0.569	0.275	0.156	692	Na <sub>2</sub> Mg <sub>3</sub> Cl <sub>8</sub> + NaMgCl <sub>3</sub> + Na <sub>3x</sub> Nd <sub>2-x</sub> Cl <sub>6</sub>
0.596	0.236	0.167	688	NaMgCl <sub>3</sub> + Na <sub>2</sub> MgCl <sub>4</sub> + Na <sub>3x</sub> Nd <sub>2-x</sub> Cl <sub>6</sub>
0.585	0.257	0.158	688	Na <sub>2</sub> MgCl <sub>4</sub> + Na <sub>6</sub> MgCl <sub>8</sub> + Na <sub>3x</sub> Nd <sub>2-x</sub> Cl <sub>6</sub>
<b>NaCl-MgCl<sub>2</sub>-PuCl<sub>3</sub> – This work</b>				
0.487	0.405	0.107	724	MgCl <sub>2</sub> + PuCl <sub>3</sub> + PuCl <sub>3</sub>
0.608	0.125	0.267	700	NaCl + Na <sub>6</sub> MgCl <sub>8</sub> + PuCl <sub>3</sub>
0.554	0.310	0.136	692	Na <sub>2</sub> Mg <sub>3</sub> Cl <sub>8</sub> + NaMgCl <sub>3</sub> + PuCl <sub>3</sub>
0.570	0.282	0.148	687	NaMgCl <sub>3</sub> + Na <sub>2</sub> MgCl <sub>4</sub> + PuCl <sub>3</sub>
0.580	0.255	0.165	688	Na <sub>2</sub> MgCl <sub>4</sub> + Na <sub>6</sub> MgCl <sub>8</sub> + PuCl <sub>3</sub>
<b>NaCl-MgCl<sub>2</sub>-PuCl<sub>3</sub> – Beneš <i>et al.</i><sup>37</sup></b>				
0.632	0.171	0.196	697	NaCl + PuCl <sub>3</sub> + Na <sub>2</sub> MgCl <sub>4</sub>
0.582	0.295	0.124	706	NaMgCl <sub>3</sub> + Na <sub>2</sub> MgCl <sub>4</sub> + PuCl <sub>3</sub>
0.521	0.389	0.090	722	MgCl <sub>2</sub> + PuCl <sub>3</sub> + NaMgCl <sub>3</sub>

sistent with the JRCMSD.<sup>31</sup> The projected liquidus surface of the ternary systems NaCl-MgCl<sub>2</sub>-NdCl<sub>3</sub> and NaCl-MgCl<sub>2</sub>-PuCl<sub>3</sub> are presented in Fig. 17 and 18, respectively.

As seen in Fig. 17 and 18, the projected liquidus surface of the NaCl-MgCl<sub>2</sub>-NdCl<sub>3</sub> and NaCl-MgCl<sub>2</sub>-PuCl<sub>3</sub> systems are similar. This is also seen in Table 10, in which the ternary equilibria are presented. Table 10 also shows that the number of ternary invariant compositions found using our thermodynamic model are different compared to those of Beneš *et al.* This is because in our model of the NaCl-MgCl<sub>2</sub> system, we used four intermediate compounds (Na<sub>6</sub>MgCl<sub>8</sub>, Na<sub>2</sub>MgCl<sub>4</sub>, NaMgCl<sub>3</sub> and Na<sub>2</sub>Mg<sub>3</sub>Cl<sub>8</sub>), whereas Beneš *et al.* used two

(Na<sub>2</sub>MgCl<sub>4</sub> and NaMgCl<sub>3</sub>). However, the compositions and temperatures of the ternary invariant equilibria predicted by Beneš *et al.* are close to compositions at which our thermodynamic model also predicts invariant equilibria.

Furthermore, the liquidus projections of the ternary systems NaCl-MgCl<sub>2</sub>-CeCl<sub>3</sub> and NaCl-MgCl<sub>2</sub>-UCl<sub>3</sub> are presented in Fig. 19 and 20, respectively. The ternary invariant equilibria shown on the liquidus projections in these figures are also listed in Table 11, along with the predicted invariant equilibria by Beneš *et al.*<sup>37</sup> Like in Table 10, the difference in the number of invariant equilibria found by Beneš *et al.* and our model is explained by the different amount of intermediate compounds present in the models. Again, like in the NaCl-MgCl<sub>2</sub>-PuCl<sub>3</sub>

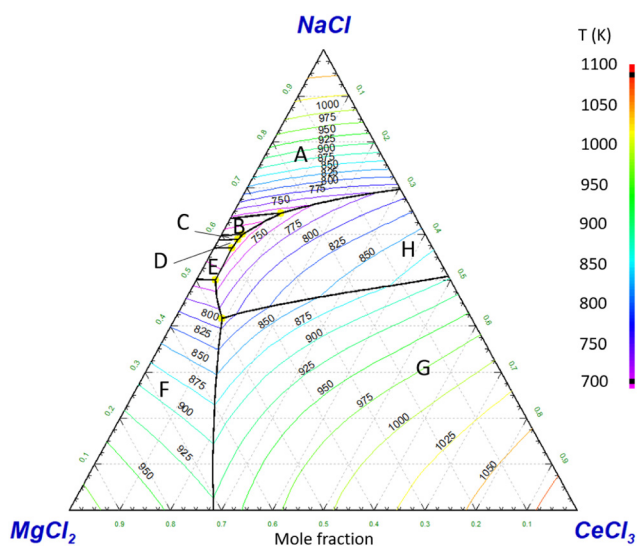


**Fig. 19** Projected liquidus surface of the NaCl-MgCl<sub>2</sub>-CeCl<sub>3</sub> system, calculated with the thermodynamic model presented in this work. Phases listed A–H on the ternary diagram are the primary crystallization phases at that composition. Phases listed are NaCl (A), Na<sub>6</sub>MgCl<sub>8</sub> (B), Na<sub>2</sub>MgCl<sub>4</sub> (C), NaMgCl<sub>3</sub> (D), Na<sub>2</sub>Mg<sub>3</sub>Cl<sub>8</sub> (E), MgCl<sub>2</sub> (F), CeCl<sub>3</sub> (G) and Na<sub>3x</sub>Ce<sub>2-x</sub>Cl<sub>6</sub> (H). The calculated ternary equilibria are presented in Table 11.

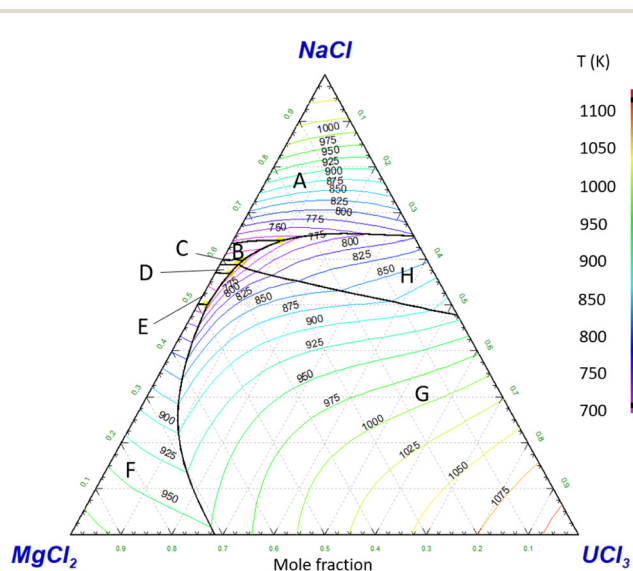


**Fig. 20** Projected liquidus surface of the NaCl-MgCl<sub>2</sub>-UCl<sub>3</sub> system, calculated with the thermodynamic model presented in this work. Phases listed A–H on the ternary diagram are the primary crystallization phases at that composition. Phases listed are NaCl (A), Na<sub>6</sub>MgCl<sub>8</sub> (B), Na<sub>2</sub>MgCl<sub>4</sub> (C), NaMgCl<sub>3</sub> (D), Na<sub>2</sub>Mg<sub>3</sub>Cl<sub>8</sub> (E), MgCl<sub>2</sub> (F), UCl<sub>3</sub> (G) and NaU<sub>2</sub>Cl<sub>7</sub> (H). The calculated ternary eutectic equilibria are presented in Table 11.



**Table 11** Calculated ternary invariant equilibria in the NaCl–MgCl<sub>2</sub>–MCl<sub>3</sub> systems (M = Ce, U)

$x(\text{NaCl})$	$x(\text{MgCl}_2)$	$x(\text{MCl}_3)$	$T$ (K)	Invariant equilibrium
<b>NaCl–MgCl<sub>2</sub>–CeCl<sub>3</sub> – This work</b>				
0.417	0.490	0.093	787	MgCl <sub>2</sub> + CeCl <sub>3</sub> + Na <sub>3x</sub> Ce <sub>2-x</sub> Cl <sub>6</sub>
0.645	0.261	0.095	733	MgCl <sub>2</sub> + Na <sub>3x</sub> Ce <sub>2-x</sub> Cl <sub>6</sub> + Na <sub>2</sub> Mg <sub>3</sub> Cl <sub>8</sub>
0.499	0.462	0.039	730	NaCl + Na <sub>6</sub> MgCl <sub>8</sub> + Na <sub>3x</sub> Ce <sub>2-x</sub> Cl <sub>6</sub>
0.570	0.394	0.036	710	Na <sub>2</sub> Mg <sub>3</sub> Cl <sub>8</sub> + NaMgCl <sub>3</sub> + Na <sub>3x</sub> Ce <sub>2-x</sub> Cl <sub>6</sub>
0.599	0.359	0.042	708	NaMgCl <sub>3</sub> + Na <sub>2</sub> MgCl <sub>4</sub> + Na <sub>3x</sub> Ce <sub>2-x</sub> Cl <sub>6</sub>
0.588	0.374	0.038	706	Na <sub>2</sub> MgCl <sub>4</sub> + Na <sub>6</sub> MgCl <sub>8</sub> + Na <sub>3x</sub> Ce <sub>2-x</sub> Cl <sub>6</sub>
<b>NaCl–MgCl<sub>2</sub>–UCl<sub>3</sub> – This work</b>				
0.639	0.260	0.101	735	MgCl <sub>2</sub> + UCl <sub>3</sub> + NaU <sub>2</sub> Cl <sub>7</sub>
0.500	0.481	0.020	733	MgCl <sub>2</sub> + NaU <sub>2</sub> Cl <sub>7</sub> + Na <sub>2</sub> Mg <sub>3</sub> Cl <sub>8</sub>
0.568	0.402	0.029	711	NaCl + Na <sub>6</sub> MgCl <sub>8</sub> + NaU <sub>2</sub> Cl <sub>7</sub>
0.597	0.360	0.043	709	Na <sub>2</sub> Mg <sub>3</sub> Cl <sub>8</sub> + NaMgCl <sub>3</sub> + NaU <sub>2</sub> Cl <sub>7</sub>
0.596	0.361	0.042	707	NaMgCl <sub>3</sub> + Na <sub>2</sub> MgCl <sub>4</sub> + NaU <sub>2</sub> Cl <sub>7</sub>
0.587	0.378	0.036	707	Na <sub>2</sub> MgCl <sub>4</sub> + Na <sub>6</sub> MgCl <sub>8</sub> + NaU <sub>2</sub> Cl <sub>7</sub>
<b>NaCl–MgCl<sub>2</sub>–UCl<sub>3</sub> – Beneš <i>et al.</i><sup>37</sup></b>				
0.637	0.251	0.112	719	NaCl + UCl <sub>3</sub> + Na <sub>2</sub> MgCl <sub>4</sub>
0.578	0.356	0.066	720	NaMgCl <sub>3</sub> + Na <sub>2</sub> MgCl <sub>4</sub> + UCl <sub>3</sub>
0.520	0.433	0.047	731	MgCl <sub>2</sub> + UCl <sub>3</sub> + NaMgCl <sub>3</sub>

system, the invariant equilibria calculated by Beneš *et al.* agree with our thermodynamic model. Additionally, when comparing the liquidus surfaces of all NaCl–MgCl<sub>2</sub>–MCl<sub>3</sub> (M = Ce, Nd, U, Pu) systems, it reinforces the notion that Nd is more accurate as a simulant for Pu than either Ce or U. The behaviour of CeCl<sub>3</sub> in the molten salt systems presented in this chapter is closer to that of UCl<sub>3</sub>, hence Ce could be used as a simulant for U instead.

## 5 Summary

We demonstrate in this work, by comparing the phase diagrams of the NaCl–MCl<sub>3</sub> and MgCl<sub>2</sub>–MCl<sub>3</sub> systems (M = Ce, Nd, U, Pu), that NdCl<sub>3</sub> is the most suitable simulant for the melting behaviour of multicomponent systems containing PuCl<sub>3</sub>, while CeCl<sub>3</sub> is most adapted for UCl<sub>3</sub>-based systems.

Furthermore, a structural investigation of the intermediate compounds in the NaCl–NdCl<sub>3</sub> and NaCl–CeCl<sub>3</sub> systems has been performed. The existence of the intermediate compound Na<sub>3x</sub>RE<sub>2-x</sub>Cl<sub>6</sub> (RE = Ce, Nd) has been found as well as the solubility limits. This solid solubility has been included in the re-assessment of the thermodynamic models. This solid solution is not included in the existing models for the systems NaCl–UCl<sub>3</sub> and NaCl–PuCl<sub>3</sub> by Yingling *et al.*<sup>35</sup> and Dumaire *et al.*,<sup>28</sup> respectively, but further experimental investigation is recommended to investigate the possible intermediate compounds Na<sub>3x</sub>An<sub>2-x</sub>Cl<sub>6</sub> (An = U, Pu) in view of the strong similarities between the actinide and lanthanide systems discussed here.

Moreover, the models for the simple binary eutectic systems MgCl<sub>2</sub>–MCl<sub>3</sub> (M = Ce, Nd, U, Pu) have been optimized based on the experimental data reported in the literature, as well as the estimated mixing enthalpies using the method of Davis and Rice. Finally, ternary extrapolations to the systems NaCl–MgCl<sub>2</sub>–MCl<sub>3</sub> (M = Ce, Nd, U, Pu) have been made and compared to values reported in the literature, showing a good

agreement between the two, confirming that in these higher order systems, NdCl<sub>3</sub> and CeCl<sub>3</sub> are the most suitable simulants for PuCl<sub>3</sub> and UCl<sub>3</sub> based salts, respectively.

## Conflicts of interest

The authors declare to have no competing financial interests or personal relationships that influence the work reported in this paper.

## Data availability

The experimental and computational data obtained in this work has been reported in the main text in Tables 2–11 and Fig. 1–20, as well as Fig. B.1–B.8 of the Appendix.

Supplementary information (SI) is available. See DOI: <https://doi.org/10.1039/d5dt01486g>.

## Acknowledgements

The authors of this paper gratefully acknowledge financial support from the ORANO group, as well as the help of L. M. T. de Geus and N. T. H. ter Veer with the synchrotron-XRD experiments. We acknowledge the European Synchrotron Radiation Facility (ESRF) for provision of synchrotron X-ray radiation facilities under proposal number MA-6356.

## References

- 1 E. Bettis, R. Schroeder, G. Cristy, H. Savage, R. Affel and L. Hemphill, The aircraft reactor experiment—design and construction, *Nucl. Sci. Eng.*, 1957, 2(6), 804–825.
- 2 J. W. McMurray, K. Johnson, C. Agca, B. R. Betzler, D. J. Kropaczek, T. M. Besmann, D. Andersson and N. Ezell,



- Roadmap for thermal property measurements of molten salt reactor systems, Oak Ridge National Lab.(ORNL), Oak Ridge, TN (United States), Tech. Rep. No. ORNL/SPR-2020/1865, 2021.
- 3 J. Latkowski, Terrapower's molten chloride fast reactor (mcftr), in *Proceedings of the Merits and Viability of Different Nuclear Fuel Cycles and Technology Options and the Waste Aspects of Advanced Nuclear Reactors, Virtual Meeting*, 2021, pp. 28–29.
  - 4 M. S. Walls and K. D. Yancey Spencer, Molten chloride reactor experiment, Idaho National Laboratory (INL), Idaho Falls, ID (United States), Tech. Rep. No. INL/MIS-23-73611, 2023.
  - 5 M. Mascaron, T. Le Meute, J. Martinet, V. Pascal, F. Bertrand and E. Merle, Study of the aramis molten salt reactor behavior during unprotected transients, in *ICAPP 2023–2023 International Congress on Advances in Nuclear Power Plants, in conjunction with 38th Korea Atomic Power Annual Conference (ICAPP 2023/KAP Conference)*, 2023, p. 2023200.
  - 6 V. Tiwari, T. Abbink, J. O. Flores, J. Flèche, C. Gueneau, S. Chatain, A. Smith, J. Martinet and C. Venard, Thermodynamic assessment of the nacl-crcl<sub>2</sub>, nacl-crcl<sub>3</sub>, and fecl<sub>2</sub>-crcl<sub>2</sub> pseudo-binary systems for describing the corrosion chemistry between molten salt fuel and steel, *Nucl. Sci. Eng.*, 2023, **197**(12), 3035–3057.
  - 7 A. Smith, E. Capelli, A. Laureau, E. Merle, J. Ocadiz-Flores and O. Beneš, Technical note regarding the selection of salt composition in WP2 (Milestone MS2)), MIMOSA project, Tech. Rep., 06 2022.
  - 8 R. A. Sharma and R. A. Rogers, Phase equilibria and structural species in NdCl<sub>3</sub> – NaCl, NdCl<sub>3</sub> – CaCl<sub>2</sub>, PrCl<sub>3</sub> – NaCl, and PrCl<sub>3</sub> – CaCl<sub>2</sub> systems, *J. Am. Ceram. Soc.*, 1992, **75**(9), 2484–2490.
  - 9 K. Igarashi, M. Kosaka, Y. Iwadate, T. Hattori and J. Mochinaga, Phase diagrams of licl-ndcl<sub>3</sub>, nacl-ndc<sub>3</sub>, and cacl<sub>2</sub>-ndcl<sub>3</sub> systems, *Denki Kagaku oyobi Kogyo Butsuri Kagaku*, 1990, **58**(5), 469–470.
  - 10 T. Sato and T. Ogawa, Phase diagram of the neodymium chloride-sodium chloride system, *J. Therm. Anal.*, 1998, **52**, 363–371.
  - 11 H. Seifert, J. Sandrock and G. Thiel, Thermochemical studies on the systems aCl/CeCl<sub>3</sub> (a = na-cs), *J. Therm. Anal.*, 1986, **31**, 1309–1318.
  - 12 F. Lissner, K. Krämer, T. Schleid, G. Meyer, Z. Hu and G. Kaindl, Die chloride Na<sub>3x</sub>M<sub>2-x</sub>Cl<sub>6</sub> (m = la-sm) und NaM<sub>2</sub>Cl<sub>6</sub> (m = nd, sm): Derivate des UCl<sub>3</sub> -typs. synthese, kristallstruktur und röntgenabsorptionsspektroskopie (xanes), *Z. Anorg. Allg. Chem.*, 1994, **620**(3), 444–450.
  - 13 G. Meyer and T. Schleid, The metallothermic reduction of several rare-earth trichlorides with lithium and sodium, *J. Less-Common Met.*, 1986, **116**(1), 187–197.
  - 14 H. T. Davis and S. A. Rice, Perturbation theory of the heats of mixing of fused salts, *J. Chem. Phys.*, 1964, **41**(1), 14–24.
  - 15 D. C. Alders, J. Vlieland, M. Thijs, R. J. M. Konings and A. L. Smith, Experimental investigation and thermo-  
dynamic assessment of the AECl<sub>2</sub> – NdCl<sub>3</sub> (AE = Sr, Ba) systems, *J. Mol. Liq.*, 2024, 123997.
  - 16 M. W. Chase Jr, NIST-JANAF thermochemical tables, *J. Phys. Chem. Ref. Data, Monogr.*, 1998, **9**, 831–834.
  - 17 R. J. M. Konings and A. Kovács, Thermodynamic properties of the lanthanide (III) halides, in *Handbook on the physics and chemistry of rare earths*, 2003, vol. 33, pp. 147–247.
  - 18 D. C. Alders, B. A. Rooijackers, R. J. Konings and A. L. Smith, Experimental investigation and thermodynamic modeling assessment of the nacl-naï-mgcl<sub>2</sub>-mg<sub>2</sub> quaternary system, *J. Phys. Chem. C*, 2025, 2726–2738.
  - 19 D. C. Alders, D. J. Cette, R. J. M. Konings and A. L. Smith, Experimental investigation and thermodynamic assessment of the AECl<sub>2</sub> – NdCl<sub>3</sub> (ae = sr, ba) systems, *Phys. Chem. Chem. Phys.*, 2024, 123997.
  - 20 H. M. Rietveld, A profile refinement method for nuclear and magnetic structures, *J. Appl. Crystallogr.*, 1969, **2**(2), 65–71.
  - 21 B. van Laar and H. Schenk, The development of powder profile refinement at the Reactor Centre Netherlands at Petten, *Acta Crystallogr., Sect. A: Found. Adv.*, 2018, **74**(2), 88–92.
  - 22 J. Rodríguez-Carvajal, Recent advances in magnetic structure determination by neutron powder diffraction, *Phys. B*, 1993, **192**, 55–69.
  - 23 K. Momma and F. Izumi, Vesta: a three-dimensional visualization system for electronic and structural analysis, *Appl. Crystallogr.*, 2008, **41**(3), 653–658.
  - 24 A. C. Scheinost, J. Claussner, J. Exner, M. Feig, S. Findeisen, C. Hennig, K. O. Kvashnina, D. Naudet, D. Prieur, A. Rossberg, *et al.*, Robl-ii at esrf: a synchrotron toolbox for actinide research, *Synchrotron Radiat.*, 2021, **28**(1), 333–349.
  - 25 J. Kieffer, V. Valls, N. Blanc and C. Hennig, New tools for calibrating diffraction setups, *Synchrotron Radiat.*, 2020, **27**(2), 558–566.
  - 26 H. Lukas, S. G. Fries and B. Sundman, *Computational thermodynamics: the Calphad method*, Cambridge University Press, 2007.
  - 27 Centre for Research in Computational Thermochemistry, “Factsage 8.2”. [Online]. Available: <https://www.factsage.com>.
  - 28 T. Dumaire, J. A. Ocadiz-Flores, R. J. M. Konings and A. L. Smith, A promising fuel for fast neutron spectrum molten salt reactor: NaCl – ThCl<sub>4</sub> – PuCl<sub>3</sub>, *Calphad*, 2022, **79**, 102496.
  - 29 J. O. Flores, R. Konings and A. Smith, Using the quasi-chemical formalism beyond the phase diagram: Density and viscosity models for molten salt fuel systems, *J. Nucl. Mater.*, 2022, **561**, 153536.
  - 30 J. A. Ocadiz Flores, B. A. Rooijackers, R. J. Konings and A. L. Smith, Thermodynamic description of the aCl-thcl<sub>4</sub> (a = li, na, k) systems, *Thermo*, 2021, **1**(2), 122–133.
  - 31 O. Beneš, Thermodynamic database on molten salt reactor systems, European Commission, Joint Research Centre, Tech. Rep., 2021.



- 32 G. van Oudenaren, J. A. Ocadiz-Flores and A. L. Smith, Coupled structural-thermodynamic modelling of the molten salt system NaCl – UCl<sub>3</sub>, *J. Mol. Liq.*, 2021, **342**, 117470.
- 33 E. Capelli and R. J. Konings, *Halides of the actinides and fission products relevant for molten salt reactors*, Elsevier, 2020.
- 34 P. Chartrand and A. D. Pelton, Thermodynamic evaluation and optimization of the LiCl – NaCl – KCl – RbCl – CsCl – MgCl<sub>2</sub> – CaCl<sub>2</sub> – SrCl<sub>2</sub> – BaCl<sub>2</sub> system using the modified quasichemical model, *Can. Metall. Q.*, 2001, **40**(1), 13–32.
- 35 J. Yingling, J. Schorne-Pinto, M. Aziziha, J. Ard, A. Mofrad, M. Christian, C. Dixon and T. Besmann, Thermodynamic measurements and assessments for licl-nacl-kcl-ucl3 systems, *J. Chem. Thermodyn.*, 2023, **179**, 106974.
- 36 A. D. Pelton, P. Chartrand and G. Eriksson, The modified quasi-chemical model: Part IV. Two-sublattice quadruplet approximation, *Metall. Mater. Trans. A*, 2001, **32**(6), 1409–1416.
- 37 O. Beneš and R. J. M. Konings, Thermodynamic evaluation of the NaCl – MgCl<sub>2</sub> – UCl<sub>3</sub> – PuCl<sub>3</sub> system, *J. Nucl. Mater.*, 2008, **375**(2), 202–208.
- 38 J. G. Darab, H. Li, J. J. Bucher, J. P. Icenhower, P. G. Allen, D. K. Shuh and J. D. Vienna, Redox chemistry of plutonium and plutonium surrogates in vitrified nuclear wastes, *J. Am. Ceram. Soc.*, 2022, **105**(11), 6627–6639.
- 39 J. C. Marra, *Cerium as a surrogate in the plutonium immobilized form*, Savannah River Site (SRS), Aiken, SC (United States), Tech. Rep. WSRC-MS-2001-00007; TRN: US0103087, 2001.
- 40 E. Sooby, A. Nelson, J. White and P. McIntyre, Measurements of the liquidus surface and solidus transitions of the NaCl – UCl<sub>3</sub> and NaCl – UCl<sub>3</sub> – CeCl<sub>3</sub> phase diagrams, *J. Nucl. Mater.*, 2015, **466**, 280–285.
- 41 A. Quemet, E. Buravand, B. Catanese, P. Huot, V. Dalier and A. Ruas, Monitoring the plutonium depletion in dissolution residues of a spent fuel solution using a surrogate and plutonium isotope ratio measurements, *J. Radioanal. Nucl. Chem.*, 2020, **326**, 255–260.
- 42 J. N. Cross, S. K. Cary, J. T. Stritzinger, M. J. Polinski and T. E. Albrecht-Schmitt, Synthesis and spectroscopy of new plutonium(III) and-(IV) molybdates: Comparisons of electronic characteristics, *Inorg. Chem.*, 2014, **53**(6), 3148–3152.
- 43 T. G. Parker, A. L. Chown, A. Beehler, D. Pubbi, J. N. Cross and T. E. Albrecht-Schmitt, Ionothermal synthesis of tetranuclear borate clusters containing f- and p-block metals, *Inorg. Chem.*, 2015, **54**(2), 570–575.
- 44 S. Delpech, C. Carrière, A. Chmakoff, L. Martinelli, D. Rodrigues and C. Cannes, Corrosion mitigation in molten salt environments, *Materials*, 2024, **17**(3), 581.
- 45 K. Goloviznina and M. Salanne, What is a good simulant for plutonium(III) in molten chloride salts?, *J. Phys. Chem. B*, 2025, **129**(30), 7826–7830.
- 46 H. J. Seifert, H. Fink and G. Thiel, Thermodynamic properties of double chlorides in the systems ACl/LaCl<sub>3</sub> (a = Na, K, Rb, Cs), *J. Less-Common Met.*, 1985, **110**(1–2), 139–147.
- 47 H. Seifert, Ternary chlorides of the trivalent early lanthanides. phase diagrams, crystal structures and thermodynamic properties, *J. Therm. Anal. Calorim.*, 2002, **67**(3), 789–826.
- 48 H. Seifert, J. Sandrock and J. Uebach, Zur stabilität von doppelchloriden in den systemen aCl/prCl<sub>3</sub> (a = Na-Cs), *Z. Anorg. Allg. Chem.*, 1987, **555**(12), 143–153.
- 49 S. Yimin, M. Xiangzhen, L. Jun, Y. Shunxiang, M. Zhisen and Q. Zhiyu, Thermodynamic assessment of DyCl<sub>3</sub> – MCl (m = Na, K, Rb, Cs) systems, *J. Rare Earths*, 2007, **25**(1), 36–41.
- 50 X. Meng, Y. Sun, S. Yuan, Z. Ma, Y. Wang and Z. Qiao, Thermodynamic optimization and calculation of the ErCl<sub>3</sub> – MCl (m = Li, Na, K, Rb, Cs) systems, *Calphad*, 2006, **30**(3), 301–307.
- 51 Z. Ma, Y. Sun, Y. Ding, Y. Wang, Z. Qiao and X. Ye, Thermodynamic calculation of the GdCl<sub>3</sub> – ACl (a = Na, K, Rb, Cs) phase diagrams based on experimental data, *Calphad*, 2006, **30**(1), 88–94.
- 52 B. Korshunov, D. Drobot, V. Bukhtiyarov and Z. Shevtsova, Vzaimodeistvie khlorida samariya (III) s khloridami natriya, kaliya, rubidiya i tsezyia, *Zh. Neorg. Khim.*, 1964, **9**(6), 1427–1430.
- 53 C. Bjorklund, J. Reavis, J. Leary and K. Walsh, Phase equilibria in the binary systems PuCl<sub>3</sub> – NaCl and PuCl<sub>3</sub> – LiCl, *J. Phys. Chem.*, 1959, **63**(10), 1774–1777.
- 54 Y. Sun, Z. Ma, Y. Ding, Y. Wang and Z. Qiao, Optimization and calculation of the EuCl<sub>3</sub> – MCl (m = Na, K, Rb, Cs) phase diagrams, *J. Solution Chem.*, 2005, **34**, 1197–1209.
- 55 J. Baglio, L. Brock and C. Struck, Thermodynamics of the NaX – DyX<sub>3</sub> (x = Cl, Br, I) molten salt systems, *Thermochim. Acta*, 2002, **386**(1), 27–34.
- 56 S. Yimin, Y. Yongxiang, H. Juan, M. Xiangzhen, G. Tianyi and Q. Zhiyu, Thermodynamic optimization and calculation of phase diagrams of YbCl<sub>3</sub> – MCl (m = Na, K, Rb, Cs), *J. Rare Earths*, 2008, **26**(4), 552–557.
- 57 J. Hu, Y. Sun, T. Gao, X. Meng, Y. Yao and Z. Qiao, Thermodynamic optimization and calculation of the HoCl<sub>3</sub> – MCl (m = Na, K, Rb, Cs) systems, *J. Phase Equilib. Diffus.*, 2008, **29**, 398–404.
- 58 H.-J. Seifert, J. Sandrock and J. Uebach, Systems NaCl/TbCl<sub>3</sub> and NaCl/DyCl<sub>3</sub>, *Acta Chem. Scand.*, 1995, **49**, 653–657.
- 59 I. Chojnacka, L. Rycerz, J. Kapala and M. Gaune-Escard, Calorimetric investigation of tmcl<sub>3</sub>-mcl liquid mixtures (m = Li, Na, K, Rb), *J. Mol. Liq.*, 2020, **319**, 113935.
- 60 J. Mochinaga and K. Irisawa, Phase diagrams of YCl<sub>3</sub> – KCl, YCl<sub>3</sub> – NaCl, and YCl<sub>3</sub> – KCl-NaCl systems, and densities of their molten mixtures, *Bull. Chem. Soc. Jpn.*, 1974, **47**(2), 364–367.
- 61 H. Seifert, H. Fink and J. Uebach, Properties of double chlorides in the systems ACl/NdCl<sub>3</sub> (a = Na-Cs), *J. Therm. Anal. Calorim.*, 1988, **33**(3), 625–632.
- 62 M. Gaune-Escard, L. Rycerz, W. Szczepaniak and A. Bogacz, Calorimetric investigation of PrCl<sub>3</sub> – NaCl and PrCl<sub>3</sub> – KCl liquid mixtures, *Thermochim. Acta*, 1994, **236**, 59–66.



- 63 A. Baev and G. Novikov, Thermodynamic investigation of alkali-metal and rare-earth chloride binary systems, *Russ. J. Inorg. Chem.*, 1960, **6**(11), 1320.
- 64 B. Korshunov, T. Ioniv and V. Kokorev, An investigation of interactions between thorium chlorides and chlorides of magnesium, calcium, cerium, aluminium, iron, niobium, tantalum and oxychloride of niobium in melts, *Izvestiya vysshikh uchebnykh zavedeniy, Tsvetnaya metallurgiya*, 1960, **6**, 114–118.
- 65 K. Nishihara, Y. Shimizu and N. Morita, Equilibrium diagram of the system  $\text{CeCl}_3 - \text{NaCl} - \text{BaCl}_2$ , *Electrochemistry*, 1950, **19**(4), 105–106.
- 66 T. Kojima, Metallurgical research on cerium metal (part 6): Equilibrium state diagram of  $\text{CeCl}_3 - \text{KCl} - \text{NaCl}$  system, *Electrochemistry*, 1951, **20**, 173–176.
- 67 I. Storonkin, O. Vasilkova and I. Kozhina, *Vestnik, Leningrad University*, 1973, vol. 4, pp. 80–83.
- 68 K. Krämer and G. Meyer, Addition und substitution von natrium in cer (iii)-chlorid:  $\text{Na}_{0,38}(\text{Na}_{0,19}\text{Ce}_{0,81})\text{Cl}_3$ , *Z. Anorg. Allg. Chem.*, 1990, **589**(1), 96–100.
- 69 G. Papatheodorou and O. Kleppa, Thermodynamic studies of binary charge unsymmetrical fused salt systems. cerium(III) chloride-alkali chloride mixtures, *J. Phys. Chem.*, 1974, **78**(2), 178–181.
- 70 I. Storonkin, I. Vasilkova, O. Grebrennikova and I. Kozhina, Thermographic and X-ray study of the  $\text{BaCl}_2 - \text{NaCl} - \text{CeCl}_3$  system, *Bull. Leningrad Univ.*, 1973, **22**, 84–88.
- 71 C. Kraus, Phase diagram of some complex salts of uranium with halides of the alkali and alkaline earth metals, Naval Research Laboratory, Tech. Rep. No. M-251 (ID: 12687930), 1943.
- 72 H. Matsuura, R. Takagi, L. Rycerz and M. Gaune-Escard, Enthalpies of mixing in molten  $\text{UCl}_3 - \text{NaCl}$  system, *J. Nucl. Sci. Technol.*, 2002, **39**(sup3), 632–634.
- 73 G. Vogel and A. Schneider, Chemie der seltenen erden in geschmolzenen alkalihalogeniden xii [1], *Inorg. Nucl. Chem. Lett.*, 1972, **8**(6), 513–521.
- 74 I.-C. Sun and I. Morozov, Vzaimodeistvie khloridov redkozemelnykh metallov s khloridami shchelochnykh i shchelochnozemelnykh metallov, *Zh. Neorg. Khim.*, 1958, **3**(8), 1914–1924.
- 75 V. Desyatnik, Y. Izmodenov, Y. Melnikov, I. Nichkov and S. Raspopin, Fusibility diagrams of systems based on magnesium and uranium chlorides, *Soviet At. Energy*, 1969, **26**(6), 634–635.
- 76 K. W. Johnson, M. Kahn and J. Leary, Phase equilibria in fused salt systems: binary systems of plutonium(III) chloride with the chlorides of magnesium, calcium, strontium and barium, *J. Phys. Chem.*, 1961, **65**(12), 2226–2229.

